Shock and Vibration 15 (2008) 101–126
IOS Press

A novel low-torque ball re-positioning scheme based on a sliding-mode ball observer for an automatic balancer system

Paul C.-P. Chao*, Chi-Wei Chiu and Kai-Teng Shih
Department of Electrical and Control Engineering, National Chiao Tung University, Hsinchu 300, Taiwan

Received 7 February 2006
Revised 2006

Abstract. A novel low-torque ball re-positioning scheme based on a sliding-mode ball observer is developed in this study with the aim to precisely reside the rolling ball inside an automatic balancer system (ABS) to its desired position – 180 degree opposite to the inherent imbalance of the rotating system which the ABS is attached to. In this way, the ABS is capable of substantially reducing radial vibrations of the rotating system for a decent balancing. For preliminary feasibility, the case of a single ball is considered in this study. The first step is to establish the dynamic model of the system, which is followed by the analysis to ensure stability of the desired ball position. The second step is to forge a sliding-mode observer for estimating on-line position and velocity of the ball. With ball estimation capability, a low-torque speed regulator that essentially generates a series of speed drops to the neighborhood of suspension resonance is proposed to overcome practical ball rolling friction for residing the ball at the desired position. The design characteristic of low-torque required for the regulator is particularly suited to most of commercial spindle motors which can only output limited torques at high speeds. Finally, simulations and experiments are conducted for a benchmark problem of optical disc drives in order to verify the effectiveness of the proposed scheme of the sliding-mode observer and the low-torque speed regulator.

Keywords: Vibration reduction, automatic balancer system (ABS), rolling friction and sliding-mode observer

1. Introduction

Excessive radial vibrations caused by the mass imbalances of high-speed rotating rotors present detrimental problems in many industrial applications. This is due to the fact that the principal rotating axis of the rotor does not coincide with its inertial axis. The corresponding distance between two axes is commonly called "imbalance." One of remedies to reduce vibrations is the application of an auto-balancer system (ABS), which mainly contains free-moving balls inside pre-designed circular races around the rotor. With the centrifugal force field generated by high-speed rotating rotor, the rolling balls are expected to settle at the angular positions that are centered around the 180 degrees opposite to the rotor imbalance, resulting in a significant reduction in radial vibrations.

Some studies have been devoted for various types of rotor systems to show the capability of ABS. Thearel [1, 2] initialized the analysis on various types of auto-balancers. It was found that the ball-type balancer is superior to the others owing to low friction, cost and ease to implement. A few studies were then conducted to further explore the capability of ball balancers. Inoue et al. [3] utilized numerical methods to analyze dynamics of a rotor/balancer system by assuming the rotor operated at constant speeds. Bövik and Högfors [4] showed that the auto-balancers were applicable to reduce both planar and non-planar vibrations of rotors. Jinnouchi et al. [5] concluded that ball

*Corresponding author. Tel.: +886 3 5131377; Fax: +886 3 5752469; E-mail: pchao@mail.nctu.edu.tw.

ISSN 1070-9622/08/$17.00

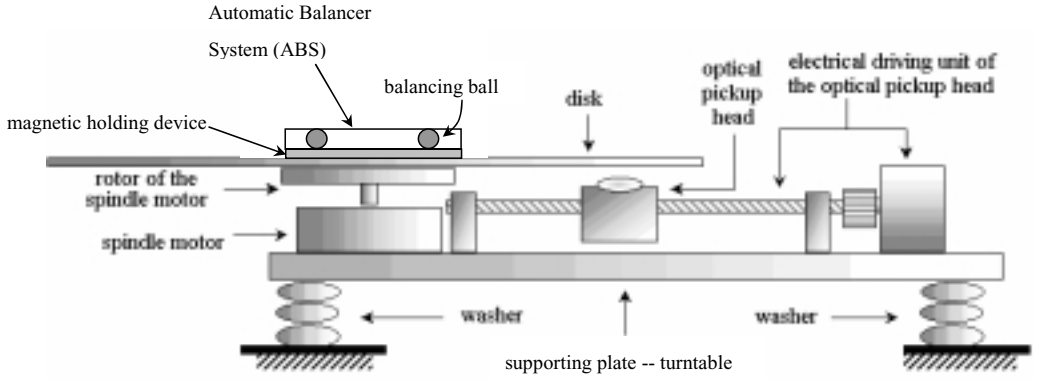

Fig. 1. Schematic of the optical pickup assembly including rotating and non-rotating parts.

balancers were able to provide excellent balancing effects above the critical speed, but led to moderate vibrations at low speeds. On the other hand, studies [6–8] are devoted to conduct stability analysis besides modeling, which is aimed to ensure ABS performance under various system parameters and operation conditions. Most recently, the ABS has been applied to optical disc drives owing to its merits of dynamic passiveness and simple structure. Some theoretical and experimental studies [9–14] were carried out to show the applicability of ABS to optical disc drives.

Among the aforementioned studies, it was found in [9,10,13] that due to the rolling friction with race flange, the ball inside the ABS settles at the position only near the desired 180 deg, rather than exactly at the position. This ball mis-positioning therefore gives rise to residual vibrations larger than desired. To further minimize the vibrations, Chao et al. [15] proposed a fuzzy speed regulator for the rotating spindles (high-speed rotors) with the aim to generate suitable circumferential inertial forces on the rolling ball inside the ABS such that the ball could be re-positioned at the desired position even with the presence of rolling friction. This fuzzy regulator is however found requiring large rotor torques while the rotor is in high-speed rotations and also a relative complicated signal processing module to be implemented, making less applicable for most commercial spindles, including those for optical disc drives. To remedy the problem, a low-torque speed regulation scheme applicable to most of commercial spindle drivers with limited torque outputs is proposed in this study, which captures the on-line ball position by a designed sliding-mode ball observer [16,17]. This regulator along with the observer is shown capable of overcoming the ball rolling friction to re-position the ball much more precisely at the position 180 degree opposite to the inherent imbalance of the rotor.

The paper is organized as follows. The dynamical model for describing the dynamics of the benchmark disc-spindle-ABS system is first established in Section 2. Section 3 presents the low-torque ball repositioning scheme, which includes the designs of the sliding-mode ball observer and the low-torque speed regulator for the rotor. Section 5 provides numerical simulations and experimental results to validate the effectiveness of aforementioned designs. Section 6 concludes the study.

2. Dynamic model

The rotating disc and spindle system in optical disc drives as shown in Fig. 1 is considered in this study for benchmarking a general rotor system. It should be noted that this developed scheme for the ABS can be generically applied to other spindle systems, like those for tool machines. The considered optical disc-drive spindle system is in fact similar to that first considered in Kang et al. [10]. The system consists of the main components that can be classified into two categories: rotating and non-rotating parts. The rotating parts constitute “the equivalent rotor” which contains the disk, magnetic holding device and the rotor of the spindle motor. The non-rotating parts constitute “the equivalent stator” which contains the foundation structure of the motor (turntable), the stator of the spindle motor, the optical pickup head, and its driving unit. The followings are assumed from the outset to facilitate the ensuing derivation of the dynamic model.

1. The equivalent rotor and stator are treated as rigid bodies.

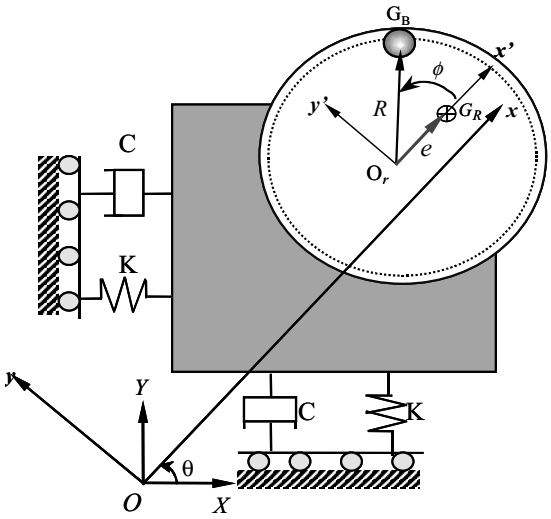

Fig. 2. Frames of reference and the mathematical model of the rotor/balancer system.

2. The flexibilities of the washers are assumed to be well captured by linear springs and dampers, denoted by k and c.
3. The vibrations in the radial direction dominate the net dynamics of the system; therefore, the motion of the system can be approximately regarded as a planar one.
4. Only one balancing ball with adequately-sized mass inside ABS is considered for preliminary feasibility study. This choice of a single ball is applicable to tool machines or optical disc drives with enough space around the rotor to accommodate an adequately-sized ball (enough mass) for counteracting the imbalance.
5. The race shapes as a perfect circle and the ball is assumed a perfect sphere. While the ball, considered as point masse, move along the race, it always keep contact with outer flange of the race, which is true in real operation at steady state due to the centrifugal field.
6. The gravitational effect on the ball is small compared to the centrifugal field.
7. No slip occurs while the ball moves since slip friction is much greater than rotational friction.
8. Since the suspension constituted by washers are much more flexible than spindle bearing's, bearing damping and stiffness forces are neglected.

Figure 2 shows the mathematical model and notations of the rotor and ABS based on the above assumptions. Only one spherical ball with mass m and radius r is considered. The following notations and coordinates are defined. G_R denotes C.G. center of the rotor whereas O_B denotes center of the balancing ball. M_R denotes the mass of the equivalent rotor while M_S is that of the equivalent stator. R represents race radius. *OXY* denotes the inertial, ground coordinate, while *Oxy* is a frame rotated in the same rotating angle as the equivalent rotor and with *Ox* stretched over G_R. The rotating angle of the rotor is denoted by θ, equivalent to the angle between *OX* and *Ox* axes. O_r is the center of the circular race, which is assumed to coincide with the rotation center of the equivalent rotor. $O_r x' y'$ is the body reference frame fixed to the equivalent rotor, which rotates with the rotor. Note that the relative distance between O and O_r indicates exactly the level of residual radial vibration, which is targeted as the physical quantity to be minimized by the ABS. e is the distance between O_r and G_R, capturing the eccentricity of the optical disc. ϕ denotes the lead angle of the ball position with respect to the current angular position of the rotor, which serves as the state variable for describing position of balancing ball.

Assuming no slip occurs between the ball and race flange, the slip friction force, denoted by F, induces a rolling moment on the ball. Acting on the ball are drag force D due to aerodynamic resistance and rolling resistant moment M_f due to ball rolling friction with race outer flange. Figure 3(a) illustrates the spatial actions of the aforementioned forces. Two accelerations, defined in the translational coordinates $O_r x' y'$, are next derived to capture the dynamics of the ball. As illustrated in Fig. 3(b), the net ball acceleration can be decomposed into tangential acceleration a_t and race flange acceleration a_w. Through the transformations bridging the inertial coordinates *OXY* and the rotating

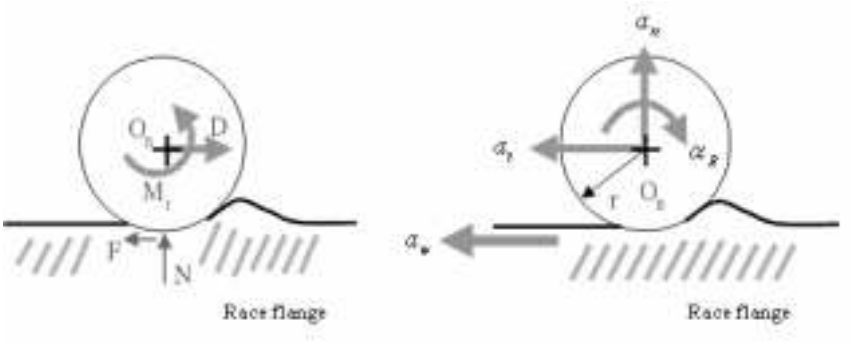

(a) (b)

Fig. 3. Free-body diagram of balancing ball. (a) Force equilibrium of the ball. (b) Definitions of ball accelerations.

coordinate $O_r x'y'$, a_t and a_w can be formulated. Balancing the forces and moments acting on the ball as shown in Fig. 3(a) leads to two equilibrium equations,

$$F - Dsgn(\dot{\phi}) = ma_t, \tag{1}$$

$$Fr - M_f[-sgn(\dot{\phi})] = I\alpha_B, \tag{2}$$

where α_B is the ball angular acceleration relative to race outer flange; I is the angular moment of inertia for the balancing ball with respect to the contact point between the rolling ball and race flange; $sgn(\bullet)$ denotes the operation of taking the sign of the considered term. Furthermore, the term $Dsgn(\dot{\phi})$ represents the drag force due to the interaction between the ball motion and surrounding fluid. This term can be assumed in an alternative form $\alpha_1 R\dot{\phi}$, the product of the adhesive coefficient, α_1, and relative velocity of the ball to the runway flange, $R\dot{\phi}$. Combining Eqs (1)–(2) for eliminating F, incorporating the pre-derived formulation of a_t and a_w into the definition of α_B, $r\alpha_B = a_W - a_t$, and utilizing the transformation between inertial frame *OXY* and rotating frame *Oxy*, the equation of motion for a single-ball balancer can be derived in terms of x and y (coordinates of the rotating frame *Oxy*) as

$$\begin{aligned}&\left(m + \frac{I}{r^2}\right) R\ddot{\phi} + mR\ddot{\theta} + m[(\ddot{y} + 2\dot{\theta}\dot{x} - \dot{\theta}^2 y + x\ddot{\theta})\cos\phi \\ &-(\ddot{x} - 2\dot{\theta}\dot{y} - \dot{\theta}^2 x - y\ddot{\theta})\sin\phi] + \alpha_1 R\dot{\phi} + \frac{M_f}{r} sgn(\dot{\phi}) = 0.\end{aligned} \tag{3}$$

The pre-derived expressions of a_t and a_w also enable derivation of the inertial forces generated by ball motion. These inertial forces are the interactive forces of the ball with the rotor system through the contacts with race wall, which can be treated as external forces for the rotor system. Then the equations of motion of the equivalent stator for a single ball can be derived easily by balancing inertial forces of the stator, interactive forces by balls, and resistant forces by suspension, which are listed as below.

$$M(\ddot{x} - 2\dot{\theta}\dot{y} - \dot{\theta}^2 x - y\ddot{\theta}) - eM_R\dot{\theta}^2 + kx + c\dot{x} - mR[(\dot{\phi} + \dot{\theta})^2\cos\phi + (\ddot{\phi} + \ddot{\theta})\sin\phi] = 0, \tag{4}$$

$$M(\ddot{y} + 2\dot{\theta}\dot{x} - \dot{\theta}^2 y + x\ddot{\theta}) + eM_R\ddot{\theta} + ky + c\dot{y} - mR[(\dot{\phi} + \dot{\theta})^2\sin\phi - (\ddot{\phi} + \ddot{\theta})\cos\phi] = 0, \tag{5}$$

where $M = M_R + M_S + m$ is the total mass of the system. In summary, Eqs (3)–(5) constitute the equations of motion that describe the general dynamics of the rotor-ABS system considered in this study.

Based on system Eqs (3)–(5), regular perturbation methods and stability techniques similar to that by Adolfsson [18] are employed to find all steady state solutions and further analyze the associated stabilities. The stability analysis is important since in practice the system only converges to stable steady state solutions; thus, it is necessary to ensure the stability of the desired ball-residing solution. The perturbation up to the first order finds two set of steady-state solutions with the ball resided at ϕ=0 and $\phi = \pi$, respectively. The solution with $\phi = \pi$ has the ball resided at the angular position 180° opposite to the rotor inherent imbalance, resulting in significant vibration reduction. Therefore, $\phi = \pi$ serves as the desired solution. Stability analysis is next conducted based on eigenvalues of the

Jacobian matrix associated with the perturbed equations of the system. It is found that as the rotor speed approaches the designated operating one, usually well above the system natural frequency; i.e. $\omega >> \omega_n = \sqrt{k/M}$, the solution with $\phi = \pi$ is the unique stable solution; in other words, another solution $\phi = 0$ is unstable. Therefore, the ABS performance of substantial radial vibration reduction is guaranteed under normal operations. The aforementioned proven stability associated with the solution $\phi = \pi$ in fact lays the foundation for the fuzzy speed regulator proposed in the next section. With proven stability for $\phi = \pi$, the regulator is allowed to be switched off after the ball is resided at the desired position since the stability reflects the physical fact that the ball resided at $\phi = \pi$ is naturally held motionless by the centrifugal field generated by the rotating rotor.

3. The ball re-positioning scheme

The stability analyses presented in the pervious section are only valid under the assumption of no rolling friction existing between the ball and race. However, it is shown by Chao et al. [13] that the ball rolling friction is inevitable in practice considering elastic deformation and surface roughness of race flange, leading to the phenomenon that the ball is only guaranteed to reside in the vicinity of the desired stable position $\phi = \pi$. To tackle the problem, the possible settling positions of the rolling ball in the presence of rolling friction are searched first, which is then followed by developing the scheme of ball re-positioning to overcome the rolling friction.

It is assumed that the ball rolls only when the circumferential inertial forces acting on the ball (generated by the centrifugal field) is greater than the resistance force due to rolling friction. In other words, at steady state as the ball stops rolling, the inertial force on the ball is smaller than or equal to the frictional moment. Based on the system equations derived in Eqs (3)–(5), the aforementioned no-rolling condition for the ball can be easily derived as

$$\left| \frac{m\omega^2 \left[mRc\omega + ec\omega M_R \cos(\phi) + eM_R \left(k - M\omega^2\right) \sin(\phi) \right]}{(k - M\omega^2)^2 + (c\omega)^2} \right| \leq \frac{M_f}{r}. \tag{6}$$

The above inequality can be solved for multiple solutions of ball positions ϕ's for a given rolling friction of M_f to render ranges of possible settling positions of the rolling ball. Figure 4(a) shows two solved ranges as opposed to levels of rolling friction at rotor speed of 10000 rpm. Figure 4(b) depicts the ranges for varied rotor rpm, while subfigure (c) is the blow-up of (b) at lower rpm for clarity. Seen from Fig. 4(a) are two ranges centered around 0 and 180 degrees, respectively. Based on the stability results obtained in the previous section, those centered around the dynamically stable solution, negative 180 degree, are the all possible settling positions with rolling friction present. Based on simple dynamic balancing rules, any settling position near but not exactly at 180 degree would result in nonzero, moderate residual vibrations, yielding an inconsistency in ABS balancing effectiveness. To deal with this inconsistency, an active mechanism, composed of a ball-position sliding-mode observer and a low-torque speed regulator, would be proposed in the following two subsections, respectively, to re-position the ball actively within the solution ranges to the desired position. The sliding-mode observer provides on-line ball position estimations, while the low-torque speed regulator operates the rotor speed in adequate times to the neighborhood of the suspension resonance, where the balls should be re-positioned much closer to the desired 180 deg due to much narrower solution ranges near the resonance (as shown in Fig. 4(c)). Note the narrower solutions near the suspension resonance, as present in Fig. 4(b,c), result from a near-zero denominator at the left hand side of Eq. (6). With more precision in ball re-positioning to 180 deg, the ABS has a fair chance to reduce radial vibration significantly.

3.1. The sliding-mode ball observer

Toward the objective of moving the ball to its desired position actively within the afore-found ball residence range by Eq. (6), the angular position of the rolling ball inside the race should be estimated in an on-line fashion. The estimated ball position could then be provided to the later-designed speed regulator to perform ball re-positioning. To this end, a nonlinear sliding-mode observer is designed in this subsection to provide real-time estimated ball positions. This observer, owing to its nature, is capable of working against external disturbance and system uncertainty.

A typical design procedure of a sliding-mode observer consists of two steps. The first step is to select a sliding surface and designate appropriate observer gains such that the observer exhibits desired behavior to estimate

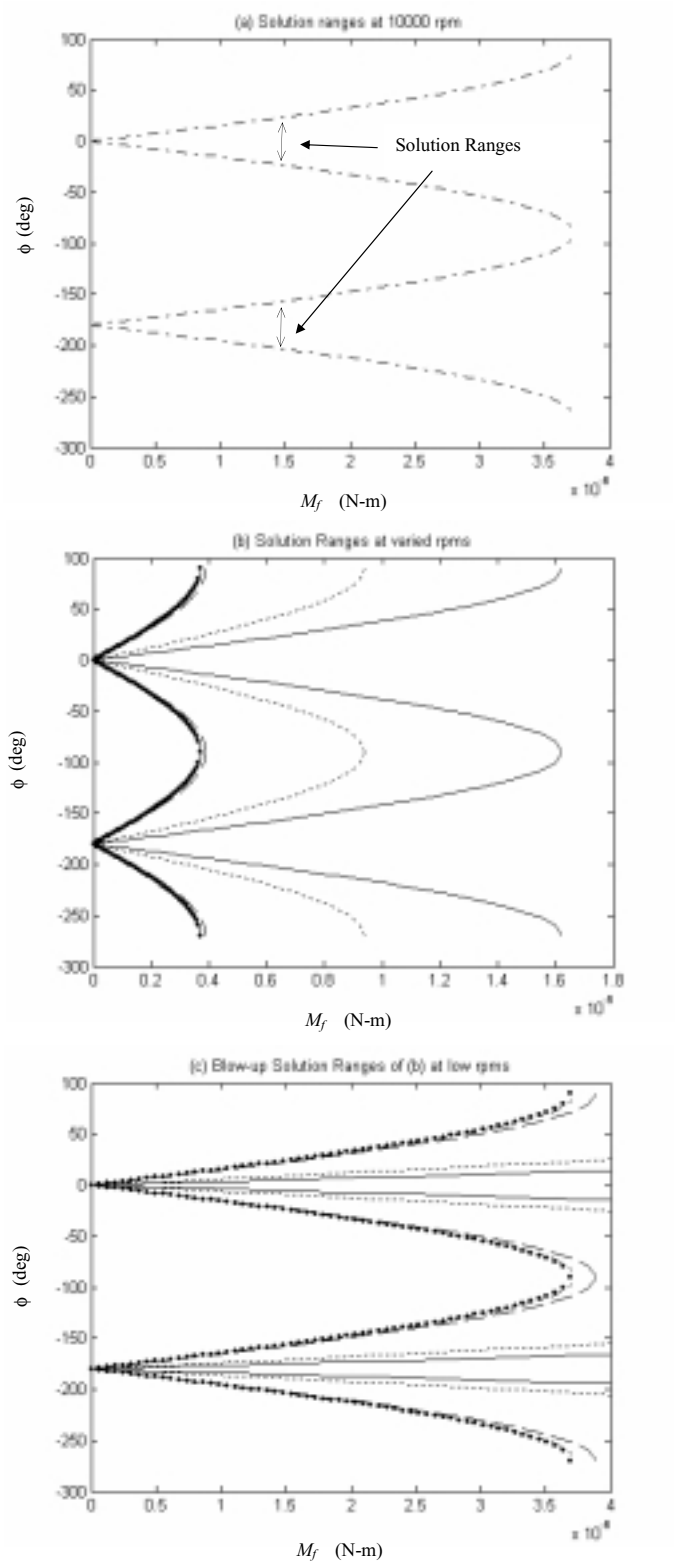

Fig. 4. The possible solution ranges of ϕ versus various rolling resistance M_f.

measurable states. The convergence in estimation errors of the measurable states would simultaneously drive convergent estimation on the remaining unavailable states by the other portion of the observer [16,17]. For the present case, the sliding-mode observer is designed to estimate current angular position and velocity of the rolling ball based on convergence in measurement errors of rotor translational motions along *OX* and *OY* directions as shown in Fig. 2; i.e., x and y. The measurements can easily be obtained by attaching two accelerometers on the stator in the respective directions. The observer is designed by first arranging the dimensional system Eqs (3)–(5) in a state-space form as

$$\begin{aligned} \dot{\mathbf{x}} &= f_1(\mathbf{x}, \boldsymbol{\varphi}), \\ \dot{\boldsymbol{\varphi}} &= f_2(\mathbf{x}, \boldsymbol{\varphi}), \end{aligned} \tag{7}$$

where $\mathbf{x} \equiv \begin{bmatrix} x\ \dot{x}\ y\ \dot{y} \end{bmatrix}^T \equiv \begin{bmatrix} x_1\ x_2\ x_3\ x_4 \end{bmatrix}$ and $\boldsymbol{\varphi} \equiv \begin{bmatrix} \phi\ \dot{\phi} \end{bmatrix}^T \equiv \begin{bmatrix} \phi_1\ \phi_2 \end{bmatrix}^T$. The detailed expressions of f_1 and f_2 are given in Appendix A. Note in Eqs (7) that the measurable states, $\mathbf{x}$, and the ones to be estimated by the observer, $\boldsymbol{\varphi}$, are separately grouped. The sliding surface is next defined as the estimation errors between measurable states $\mathbf{x}$ and the estimates offered by the observer $\hat{\mathbf{x}}$, i.e.,

$$\mathbf{s} = \begin{bmatrix} s_1\ s_2\ s_3\ s_4 \end{bmatrix}^T \equiv \hat{\mathbf{x}} - \mathbf{x}. \tag{8}$$

The siding-mode observer is then designed to comprise

$$\dot{\hat{\mathbf{x}}} = \hat{f}_1(\hat{\mathbf{x}}, \hat{\boldsymbol{\varphi}}) - \mathbf{L}_x\mathbf{s} - \mathbf{K}_x sgn(\mathbf{s}), \tag{9a}$$

$$\dot{\hat{\boldsymbol{\varphi}}} = \hat{f}_2(\hat{\mathbf{x}}, \hat{\boldsymbol{\varphi}}) - \mathbf{L}_\phi\mathbf{s} - \mathbf{K}_\phi sgn(\mathbf{s}), \tag{9b}$$

where $\hat{f}$'s are the estimated model of f's pre-defined in Appendix A; $\mathbf{L}$'s and $\mathbf{K}$'s are gain matrices to be designed; and

$$sgn(\mathbf{s}) = \begin{bmatrix} sgn(s_1)\ sgn(s_2)\ sgn(s_3)\ sgn(s_4) \end{bmatrix}^T. \tag{10}$$

The terms $\mathbf{L}_x\mathbf{s}$ and $\mathbf{L}_\phi\mathbf{s}$ in Eqs (9) provide linear error-convergences outside the sliding surface, while $\mathbf{K}_x sgn(\mathbf{s})$ and $\mathbf{K}_\phi sgn(\mathbf{s})$ generate switching error-convergence efforts inside the sliding surface. It can be conceived from Eq. (8) and the term "$\mathbf{K}_\phi sgn(\mathbf{s})$" in Eq. (9b) that estimations of the non-measurable states $\boldsymbol{\varphi}$ are driven by estimation errors of the measurable states, $(\hat{\mathbf{x}} - \mathbf{x})$. The dynamics of estimation errors by the observer can be captured by subtracting Eq .(9) from Eq. (7), yielding

$$\dot{\tilde{\mathbf{x}}} = \Delta f_1(\hat{\mathbf{x}}, \hat{\varphi}) - \mathbf{L}_x\mathbf{s} - \mathbf{K}_x sgn(\mathbf{s}), \tag{11a}$$

$$\dot{\tilde{\varphi}} = \Delta f_2(\hat{\mathbf{x}}, \hat{\varphi}) - \mathbf{L}_\phi\mathbf{s} - \mathbf{K}_\phi sgn(\mathbf{s}), \tag{11b}$$

where

$$\tilde{\mathbf{x}} \equiv \hat{\mathbf{x}} - \mathbf{x},\ \tilde{\varphi} \equiv \hat{\varphi} - \boldsymbol{\varphi},\ \Delta f_1 \equiv \hat{f}_1 - f_1,\ \text{and}\ \Delta f_2 \equiv \hat{f}_2 - f_2.$$

Following the standard procedure of sliding-mode observer design, one can use the simple forms of $\mathbf{L}_x$ and $\mathbf{K}_x$ as

$$\mathbf{L}_x = \begin{bmatrix} l_x & 0 & 0 & 0 \\ 0 & l_x & 0 & 0 \\ 0 & 0 & l_x & 0 \\ 0 & 0 & 0 & l_x \end{bmatrix} \text{ and } \mathbf{K}_x = \begin{bmatrix} k_x & 0 & 0 & 0 \\ 0 & k_x & 0 & 0 \\ 0 & 0 & k_x & 0 \\ 0 & 0 & 0 & k_x \end{bmatrix} \tag{12}$$

with large l_x and k_x to reach the convergence of $\tilde{\mathbf{x}} \to 0$. However, due to the complex nonlinearity involved in the term Δf_1 in Eq. (11), which lays great difficulty in determining values of l_x and k_x, the standard procedure of sliding-mode observer design cannot be employed herein to determine the observer gains of l_x and k_x. To solve this problem, the error Eq. (11a–b) are simplified by only considering the first linear terms of Δf_1 and Δf_2, yielding the approximate model of

$$\dot{\tilde{\mathbf{x}}} = \mathbf{F}_{11}\tilde{\mathbf{x}} + \mathbf{F}_{12}\tilde{\boldsymbol{\varphi}} - \mathbf{L}_x\mathbf{s} - \mathbf{K}_x sgn(\mathbf{s}), \tag{13a}$$

$$\dot{\tilde{\boldsymbol{\varphi}}} = \mathbf{F}_{21}\tilde{\mathbf{x}} + \mathbf{F}_{22}\tilde{\boldsymbol{\varphi}} - \mathbf{L}_{\phi}\mathbf{s} - \mathbf{K}_{\phi}sgn(\mathbf{s}), \tag{13b}$$

where

$$\mathbf{F}_{11} = \frac{\partial f_1}{\partial \mathbf{x}}, \mathbf{F}_{12} = \frac{\partial f_1}{\partial \boldsymbol{\varphi}}, \mathbf{F}_{21} = \frac{\partial f_2}{\partial \mathbf{x}}, \mathbf{F}_{22} = \frac{\partial f_2}{\partial \boldsymbol{\varphi}}. \tag{14}$$

The detailed expressions of $\mathbf{F}_{ij}$'s are given in Appendix B. Considering the linearized model in Eqs (13), the convergence condition for $\tilde{\mathbf{x}} \rightarrow 0$ based on theory of sliding-mode observer can be derived as

$$\mathbf{s}^T\dot{\mathbf{s}} = \tilde{\mathbf{x}}^T\left(\mathbf{F}_{11}\tilde{\mathbf{x}} + \mathbf{F}_{12}\tilde{\varphi} - \mathbf{L}_x\tilde{\mathbf{x}} - \mathbf{K}_x sgn(\tilde{\mathbf{x}})\right) < 0. \tag{15}$$

From the structure of the above condition, one can set the gains of $\mathbf{L}_x$ large enough to stabilize the eigenvalues of $(\mathbf{F}_{11} - \mathbf{L}_x)$, while also set the gains of $\mathbf{K}_x$ large enough to let the term $\mathbf{K}_x sgn(\tilde{\mathbf{x}})$ suppress the coupling term $\mathbf{F}_{12}\tilde{\boldsymbol{\varphi}}$. The corresponding lower limits of gains in $\mathbf{L}_x$ and $\mathbf{K}_x$ for satisfying Eq. (15) can be determined with expressions of $\mathbf{F}_{11}$ and $\mathbf{F}_{12}$ in Appendix B and reasonable assumptions on ranges of states during spindle operation. Since the process of deriving these limits is straightforward and tedious, they are not shown herein. Note that the gains of $\mathbf{L}_x$ and $\mathbf{K}_x$ are often and should be over-designed to have robustness for the observer. The next step is to determine the gain matrices associated with the unavailable states to estimate; i.e., $\mathbf{K}_{\phi}$ and $\mathbf{L}_{\phi}$. As $\tilde{\mathbf{x}}$ approaching zeros to satisfy condition (15), combination of Eqs (13) leads to

$$\dot{\tilde{\boldsymbol{\varphi}}} = \left(\mathbf{F}_{22} - \mathbf{K}_{\phi}\mathbf{K}_x^{-1}\mathbf{F}_{12}\right)\tilde{\boldsymbol{\varphi}}. \tag{16}$$

As long as the matrix $\left(\mathbf{F}_{22} - \mathbf{K}_{\phi}\mathbf{K}_x^{-1}\mathbf{F}_{12}\right)$ in Eq. (16) is Hurwitz like a time-variant linear system, the estimation error on the balancing ball $\tilde{\phi}$ goes to zero eventually. This can be accomplished by designing appropriate gains in $\mathbf{K}_{\phi}$.

A special design procedure for determining $\mathbf{K}_{\phi}$ is proposed to ensure convergence of $\tilde{\boldsymbol{\varphi}} \rightarrow 0$ and further an easy access on the convergence rate. The procedure starts with putting $\mathbf{K}_{\phi}\mathbf{K}_x^{-1}$ to be in the form of

$$\mathbf{K}_{\phi}\mathbf{K}_x^{-1} = \begin{bmatrix} a_1 & 1 \\ 0 & a_2 \end{bmatrix}\begin{bmatrix} 0 & N_{11} & 0 & N_{12} \\ 0 & N_{21} & 0 & N_{22} \end{bmatrix}, \tag{17}$$

where N_{ij}'s satisfies

$$\begin{bmatrix} 0 & N_{11} & 0 & N_{12} \\ 0 & N_{21} & 0 & N_{22} \end{bmatrix}\mathbf{F}_{12} = \mathbf{I}_{2\times 2}, \tag{18}$$

and a's are to be assigned. Note that with the special structure of $\mathbf{F}_{12}$ as shown in Appendix B – zero entries in the first and third rows, N_{ij}'s in Eq. (18) can be easily solved for a given $\mathbf{F}_{12}$; then $\mathbf{K}_{\phi}$ can be determined based on Eq. (17) with pre-designed $\mathbf{K}_x$. Incorporating Eq. (17) into system Eq. (16), one yields

$$(\mathbf{F}_{22} - \mathbf{K}_{\phi}\mathbf{K}_x^{-1}\mathbf{F}_{12}) = \begin{bmatrix} -a_1 & 0 \\ \frac{\partial p_3}{\partial \phi_1} & \frac{\partial p_3}{\partial \phi_2} - a_2 \end{bmatrix}, \tag{19}$$

where the terms $\frac{\partial p_3}{\partial \phi_1}$ and are time-varying and given in Appendix B. Based on the particular structure of the matrix in Eq. (19), the eigenvalues of the system (16) are $-a_1$ and $\left(\frac{\partial p_3}{\partial \phi_2} - a_2\right)$. At this stage, one can assign large values of a_1 and a_2 to enforce the matrix in Eq. (19) as near time-invariant and simultaneously lead to the desired speed of convergence for error estimation of the balancing ball $\tilde{\phi}$, even though the matrix in Eq. (19) contains time-varying terms $\frac{\partial p_3}{\partial \phi_1}$ and $\frac{\partial p_3}{\partial \phi_2}$. With designated a_1 and a_2, $\mathbf{K}_{\phi}$ can be determined using Eqs (17)–(18) with pre-designed $\mathbf{K}_x$.

It is pertinent to note at this point that the afore-proposed observer is forged based upon the linearized part of the subsystem due to the fact that the system possesses complex nonlinearity that makes the observer design based on the original nonlinear system almost impossible. With large-enough gains inside the matrices $\mathbf{K}_{\phi}$ and $\mathbf{L}_{\phi}$, even though the observer is designed from the linear part of the system, it still stands a fair chance to render robust convergence of estimation.

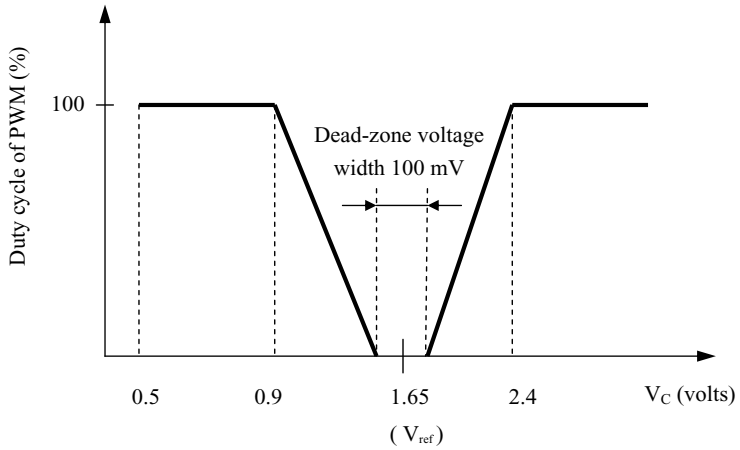

Fig. 5. The duty cycle of PWM signal driven by control signal Vc in TA8493F.

3.2. The low-torque speed regulator

With estimation capability of ball position based on the previously sliding-mode observer, a low-torque rotor speed regulator is forged in this subsection to reposition the ball at the desired position. The design goal of low torque is particularly suited to most of commercial spindle motors which owns specific driving framework and only provides limited torque outputs at high spindle speeds. A common realistic spindle system consists of a driver IC, the circuit board and spindle motor. One of mostly-seen commercial driver ICs, TA8493F from TOSHIBA Corporation, is employed in this study to implement the low-torque rotor speed regulator. The driver of TA8493F is specifically designed for driving three-phase brushless DC spindle motors in optical disc drives. TA8493F is powered by a bias in five volts and output three-phase Pulse Width Modulation (PWM) signals to drive the spindle motor. The rotating speed of spindle motor then depends on the duty cycle of the PWM signal which is adjusted by a control signal in a DC voltage, Vc. Figure 5 shows the relationship between the control signal, Vc, and the duty cycle of PWM. It can be noted from this figure that as the control signal Vc is designated out of the range bounded by [($V_{\rm ref} - 0.75$), ($V_{\rm ref} + 0.75$)] where $V_{\rm ref}$ is 1.65 volts, the PWM duty cycle is in 100%, which leads to the fastest rotating speed of the spindle motor that the driver TA8493F can achieve. On the other hand, if Vc is designated within the two ranges having oblique lines in Fig. 5, the corresponding PWM duty cycle as indicated by the oblique lines would be applied and provided to the spindle motor to accelerate or decelerate to a steady-state rotating speed. Note that the spindle reaches its steady-state speed as the torque induced by the designated PWM duty cycle is in an equilibrium with friction and air drag on the rotor system, including mainly the disc and spindle for optical disc drives. The relation between PWM duty cycle and the steady-state spindle speed can be identified through a number of easy experimental spindle runs. Using the identified relation and Fig. 5, one can further understand the relation between the control signal Vc and the steady-state spindle speed. With the relation, the spindle speed can somehow be tuned by designating Vc to a certain value in the ranges with oblique lines in Fig. 5. Finally, if Vc is assigned in the deadzone of 100 mV, as indicated in Fig. 5, the spindle would be gradually decelerated to zero speed.

To the aim of re-positioning the balancing ball more precisely to the desired angular position in ABS, a low–torque speed regulation scheme is fostered by taking advantages of the dynamic characteristics of the system and the aforementioned working principle of the driver TA8493F. Based on the previous analysis related to Eq. (6) and the results presented in Fig. 4, operating the rotor speed near the first natural frequency (resonance) of the suspension system would result in much more narrow ball residing ranges, then leading to ball steady-state positions much closer to desired 180 deg. In result, tuning the rotor speed to the neighborhood of suspension resonance helps greatly the rolling ball in ABS to overcome the rolling friction and then being re-positioned at the desired 180 degree. In this way, there is no need of large driving power from the driver to change spindle speed as required by the work in [15], while one needs only to tune the spindle speed near the first resonance frequency in a realizable way provided by the commercial driver to re-position the balancing ball. It is planned that if the ball position detected by the sliding-mode

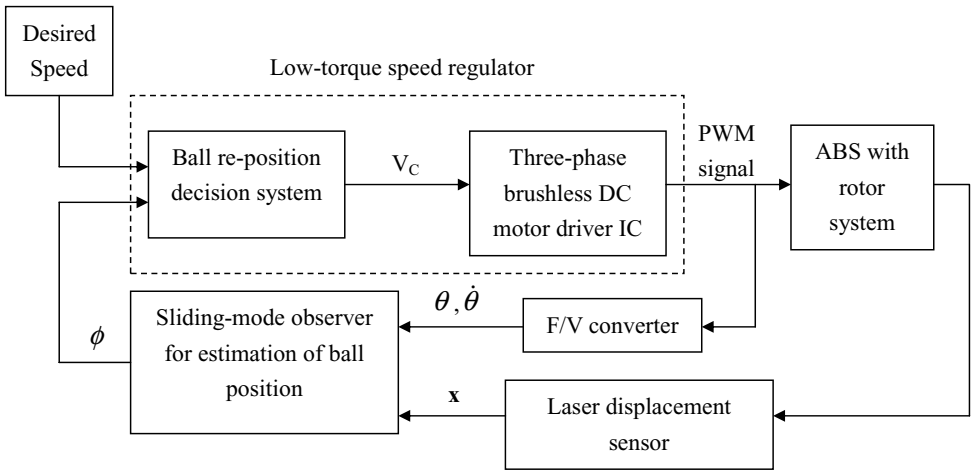

Fig. 6. Block diagram of the overall ball re-positioning scheme.

observer is not at the desired position, 180 deg opposite to the inherent imbalance of the disc-spindle-ABS system, as the spindle reaches its target operation speed, the spindle speed is forced to experience a series of speed drops to the neighborhood of the first resonance frequency of the suspension system by tuning the control signal Vc for the driver TA8493F to the value that corresponds to the low PWM duty cycle leading to the spindle speed around the first suspension resonance of 1300 rpm, as shown in Fig. 5. It is expected that the excessive vibrations caused by the resonance would re-roll the ball to the desired 180 degree. After the sudden drops, the spindle speed is recovered to the operational by re-assigning Vc to corresponding value in Fig. 5. The aforementioned speed regulation scheme is summarized below.

1. Activate the spindle rotation to the target operation speed with Vc set to the corresponding value in Fig. 5.
2. With the rolling ball settled to its steady-state angular position, check if the ball is at the desired position (180 deg opposite to the inherent imbalance) via the sliding-mode ball observer. If the ball is at the desired 180 deg, then one can terminate the speed regulation; otherwise, proceed to the next step.
3. Tune the control signal to that corresponding to the spindle speed being approximately the first resonance frequency (around 1300 rpm) for a short period of time, and then recover to the target operation spindle speed.
4. Re-examine if ball settles at the desired 180 degree. If not, repeat step 3 until the ball resides at the 180 degree; otherwise, terminate the speed regulation process.

With the sliding-mode ball observer and the low-torque speed regulation scheme successfully designed, a block diagram is depicted herein as shown in Fig. 6 to illustrate the mechanism of the overall ball re-positioning scheme. It is shown by this figure that as the disc-spindle-ABS system in rotations, a frequency-to-voltage (F/V) converter is employed to detect the spindle speed based on driver PWM signals, and also laser sensors to measure translational vibrations in X and Y directions. The measurements from the converter and sensors are fed into the sliding-mode observer for on-line estimation on the ball position. The estimated ball position is compared with the desired ball position, 180 deg, by the low-torque speed regulator, and then it takes the difference to initiate a series of drops in spindle speed via the driver and its PWM signals to the disc-spindle-ABS system. In this way, after a series of speed drops of the spindle, the rolling ball inside the ABS is expected to have a fair chance to be located at the desired position of 180 degree at steady state.

It is pertinent to note at this point that commercial disc drives with well-developed washers are capable of sustaining short-period large vibrations each time induced by the proposed low-torque scheme. However, large vibrations in an extended period of time may shorten washer lives due to fatigue. To minimize fatigue effects, one can re-design washers to extend lives, or choose a better rotor speed – instead of but near the resonance – for re-positioning the balls. Based on previous analysis, the results of which are integrally presented in Fig. 4(b,c), the aforementioned chosen operation rotor speed could result in less vibrations amplitude than resonance and at the same time lead to a narrow-enough ball residing range to re-start rolling of the balls that are already stopped at higher rpms. In this way, the lives of the washers can also be extended.

Table 1
Applied system parameters

Mass of stator, M_S	105 g
Mass of rotor, M_R	49.5 g
Mass of ball, m	0.3 g
Ball radius, r	1.5 mm
Race radius, R	16.5 mm
Suspension stiffness,k	3000 N/m
Damping, c	0.03 N-sec/m
C.G. eccentricity, e	0.04 mm
Adhesive coefficient, α_1	5×10^{-3} Ns/m^2
Rolling friction moment, M_f	1.5×10^{-6} N-m

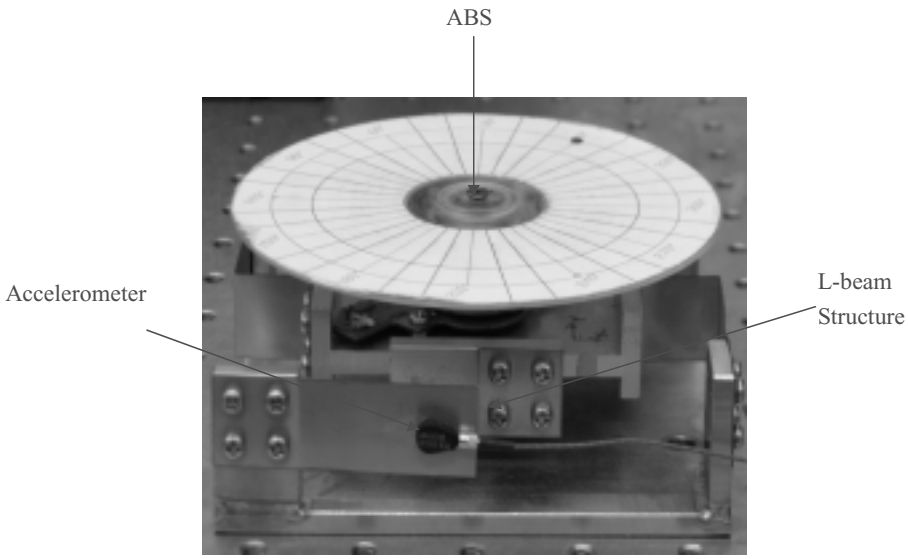

Fig. 7. Photo of the experimental disc-spindle-ABS system.

4. Numerical simulations

Numerical simulations on the disc-spindle-ABS system equipped with the sliding ball observer and the speed regulator previously designed in Sections 3.1 and 3.2, respectively, are carried out in this section to choose appropriate parameters for the sliding-mode ball observer (observer gains). The system parameters other than the observer gains are specified as those of a practical spindle-disc-ABS system specifically designed and manufactured in the laboratory, as shown in Fig. 7, for later comparison with experimental data. This experiment system includes a circular race with a ball inside, a spindle motor powered by a driver IC, an L-beam-type motor-supporting structure and two accelerometers. The L-beam base structure plays roles of damping washers in applications, realizing isotropic damping and stiffnesses of damping washers. All parameters of the aforementioned practical spindle-disc-ABS system are calibrated and listed in Table 1. With the system parameters in hand, observer gains are next chosen to reach fast error convergence of the observed ball position, as prescribed by $\tilde{\boldsymbol{\varphi}}$ in Eq. (16), within reasonable time spans. Based on theory of the sliding-mode observer, the convergence of observation error is primarily affected by four parameter matrices $\{\mathbf{L}_x, \mathbf{K}_x, \mathbf{K}_\phi, \mathbf{L}_\phi\}$, where the former two influence the convergence of measurable states, while the latter two dictate the unmeasurable states to be observed, which in the present study are ball position and velocity. With the matrices $\{\mathbf{L}_x, \mathbf{K}_x\}$ already pre-specified as diagonals with nonzero diagonal entries $\{l_x, k_x\}$ in Eq. (12), the first step of choosing observer gains is to find appropriate gain values of $\{l_x, k_x\}$. It is found based on a number of simulations with varied $\{l_x, k_x\}$ (which are not shown herein for presentation brevity) that $\{l_x, k_x\}$ affect only the convergence of the measurable states, the translational motions of the system (x and y). The speed of

Table 2
Trial gains for the sliding-mode ball observer

	l_x	k_x	a_1	a_2
Case 1	460	4	0.1	1
Case 2	460	4	1	1
Case 3	460	4	10	1
Case 4	460	4	1	4
Case 5	460	4	1	40

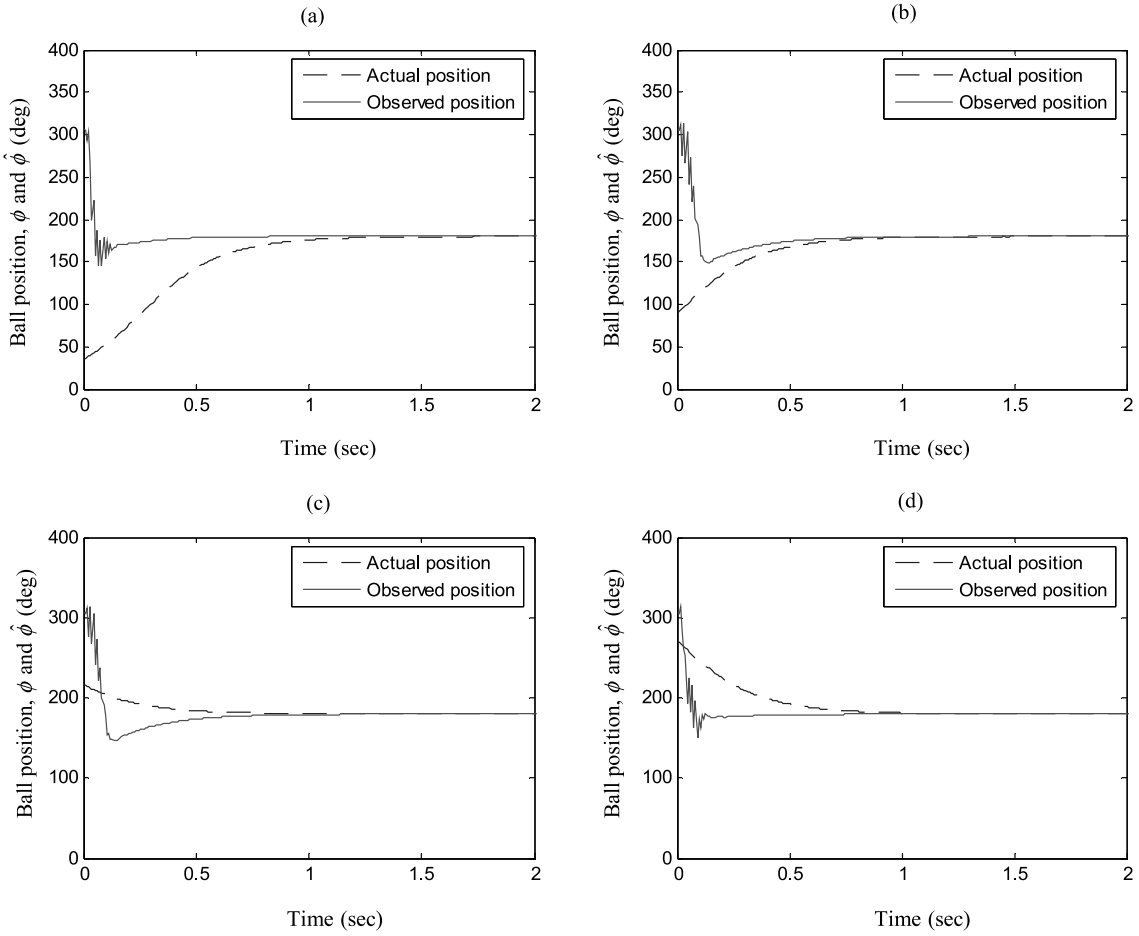

Fig. 8. Observed ball position based on the designed sliding-mode ball observer with $l_x = 460$, $k_x = 4$, $a_1 = 0.1$, $a_2 = 1$ and initial ball position at (a) 36°, (b) 90°, (c) 216° and (d) 270°.

the convergence can easily be tuned to the desireds by increasing values of $\{l_x, k_x\}$. Further found is that one can generically assign l_x and k_x to be above 460 and 4, respectively, for a satisfactory convergence of x and y.

With observer gains $\{l_x, k_x\}$ decided, the remaining task would be the determination of $\{\mathbf{K}_\phi, \mathbf{L}_\phi\}$ to tune the convergence speed of observation for unavailable states, i.e., ball position and velocity. It was offered by the design procedure presented integrally via Eqs (17)–(19) in the end of Section 3.1 that the tunings on $\{\mathbf{K}_\phi, \mathbf{L}_\phi\}$ can be transformed into those via a_1 and a_2 defined in Eq. (19). Assignments of a_1 and a_2 directly control the eigenvalues of the convergence speed of estimation on ball displacement and velocity. Table 2 lists the combinations with varied a_1 and a_2 in five cases of simulations to choose suitable observer gains for a satisfactory convergence of ball displacement and velocity. The first three cases are designated to determine a_1 while the last two cases are for a_2. Figures 8–12 depict corresponding actual and observed ball responses under various initial ball conditions. It can be

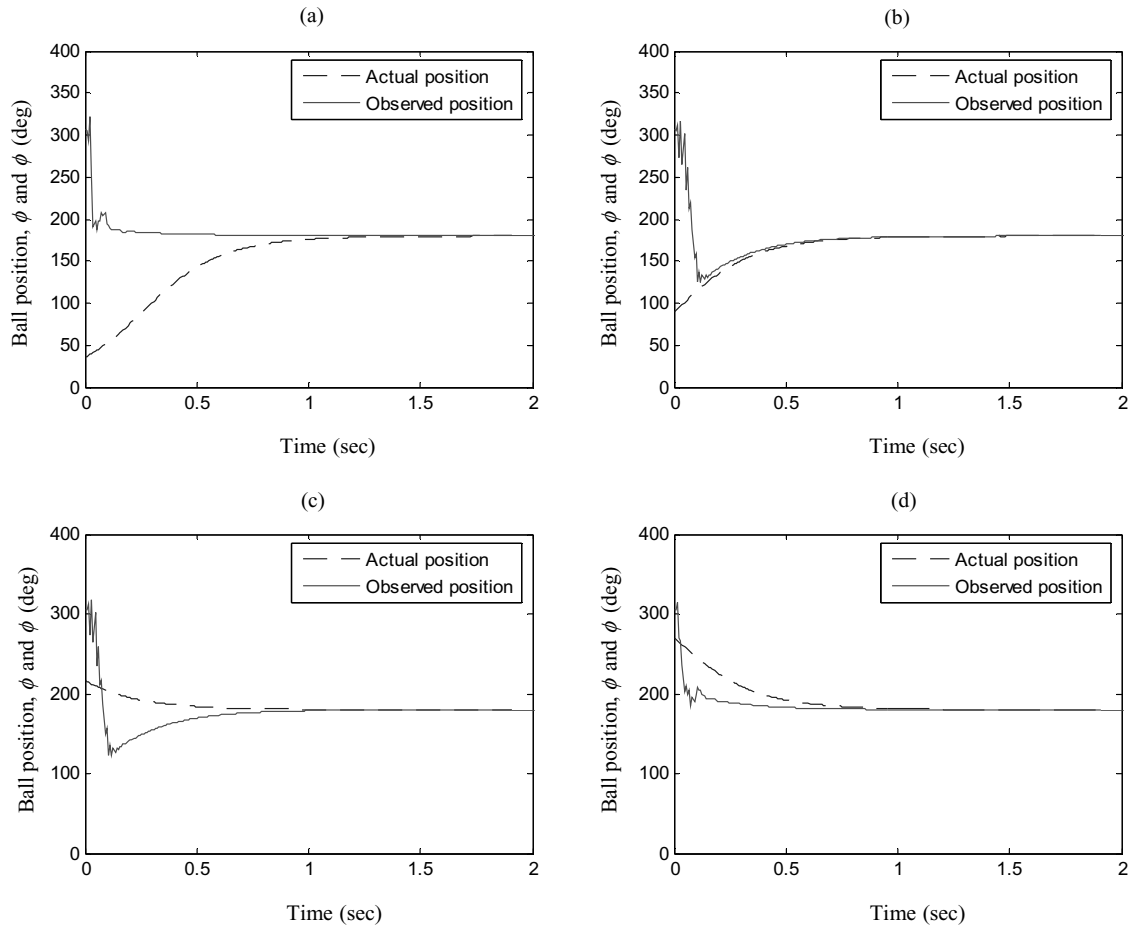

Fig. 9. Observed ball position based on the designed sliding-mode ball observer with $l_x = 460$, $k_x = 4$, $a_1 = 1$, $a_2 = 1$ and initial ball position at (a) 36°, (b) 90°, (c) 216° and (d) 270°.

seen from the first three figures (Figs 8–10) that a larger gain of a_1 leads to a generically faster observation speed, as comparing the responses with $a_1 = 0.1$ to that with $a_1 = 1$. However, a much larger gain of $a_1 = 10$ induce serious chattering phenomenon in the transient periods, as shown in Fig. 10. Therefore based on all the responses in Figs 8–10, the best gain of a_1 is $a_1 = 1$. With a_1 fixed to the chosen value, a_2 is varied to 4 and 40 for two different cases with the aim to find the suitable gain value of a_2. The simulated responses are depicted in Figs 11–12. A general comparison among Figs 9, 11 and 12 reveals that the increase of a_2 from 1 to 4 induces little difference in the characteristics of the responses despite slight chattering appears, but the increase of a_2 from 1 to 40 introduce severe chattering in transient responses as shown in Fig. 12. Conclusively speaking, the gain of a_2 can be chosen as 1 or 4 for a satisfactory performance of the sliding-mode observer.

5. Experimental results

In addition to the numerical simulations presented in the previous section, experimental studies are conducted herein to validate the effectiveness of the designed sliding-mode ball observer and accompanied speed regulator for re-positioning the ball. The experiment setup is schematically shown in Fig. 13. The experimental disc-spindle-ABS system employed are the same as that first established in [13] and shown in Fig. 13, which consists of an ABS, a test disk, a spindle motor accompanied with a driving circuit, the motor supporting structure, two accelerometers

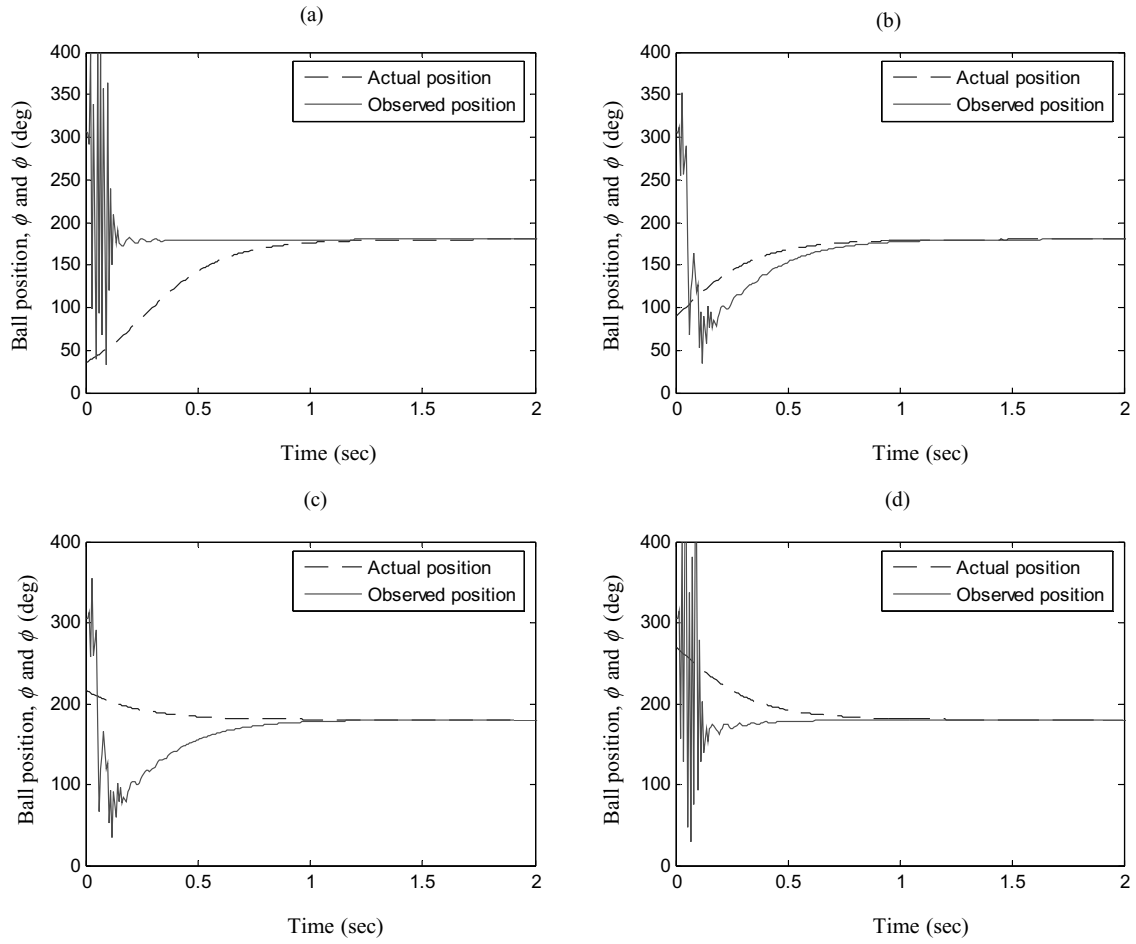

Fig. 10. Observed ball position based on the designed sliding-mode ball observer with $k_x = 460$, $k_x = 4$, $a_1 = 10$, $a_2 = 1$ and initial ball position at (a) 36°, (b) 90°, (c) 216° and (d) 270°.

for measuring translational motions, and a stroboscope accompanied with a CCD camera to capture ball positions. For a steel race used for the present study, the rolling friction is identified as 1.5×10^{-6} N-m [9]. In addition, (1) a frequency-to-voltage (F/V) converter used to provide on-line rotor speed, (2) current transducers (LTS 6-NP) for obtaining output torque by the motor, and (3) a DSP module (dSPACE1103) for implementing controller/observer algorithms with sampling frequency of 0.5 mini-second and function of filtering the noises in 60 Hz from power source are particularly employed in this study. The target operation speed is set as 2600 and 9000 rpm. The driver is tuned for a short-time speedup. The experimental study consist mainly of two parts: (1) validating the theoretical effectiveness of proposed sliding-mode observer presented in Section 3.1; (2) re-positioning the ball following the speed regulation scheme proposed in the end of Section 3.2.

5.1. Validating observer performance

Experiments are conducted for ensuring that the designed ball observer is capable of estimating states ϕ and $\mathbf{x}$ by estimates $\hat{\phi}$ and $\hat{\mathbf{x}}$ in a short period of time. Figure 14 present theoretical and experimental responses of ball angular displacement in Fig. 14(a) up to the steady state when the ball is resided to the desired angular position, 180 degree opposite to the inherent imbalance of the spindle-disc-ABS system, and also the translational displacements and velocities of the spindle-disc-ABS system along X and Y directions in Fig. 14(b–i). Note that Fig. 14(c,e,g,i) are the enlarged local responses at steady state of Fig. 14(b,d,f,h), respectively, for a clearer view on the estimated X

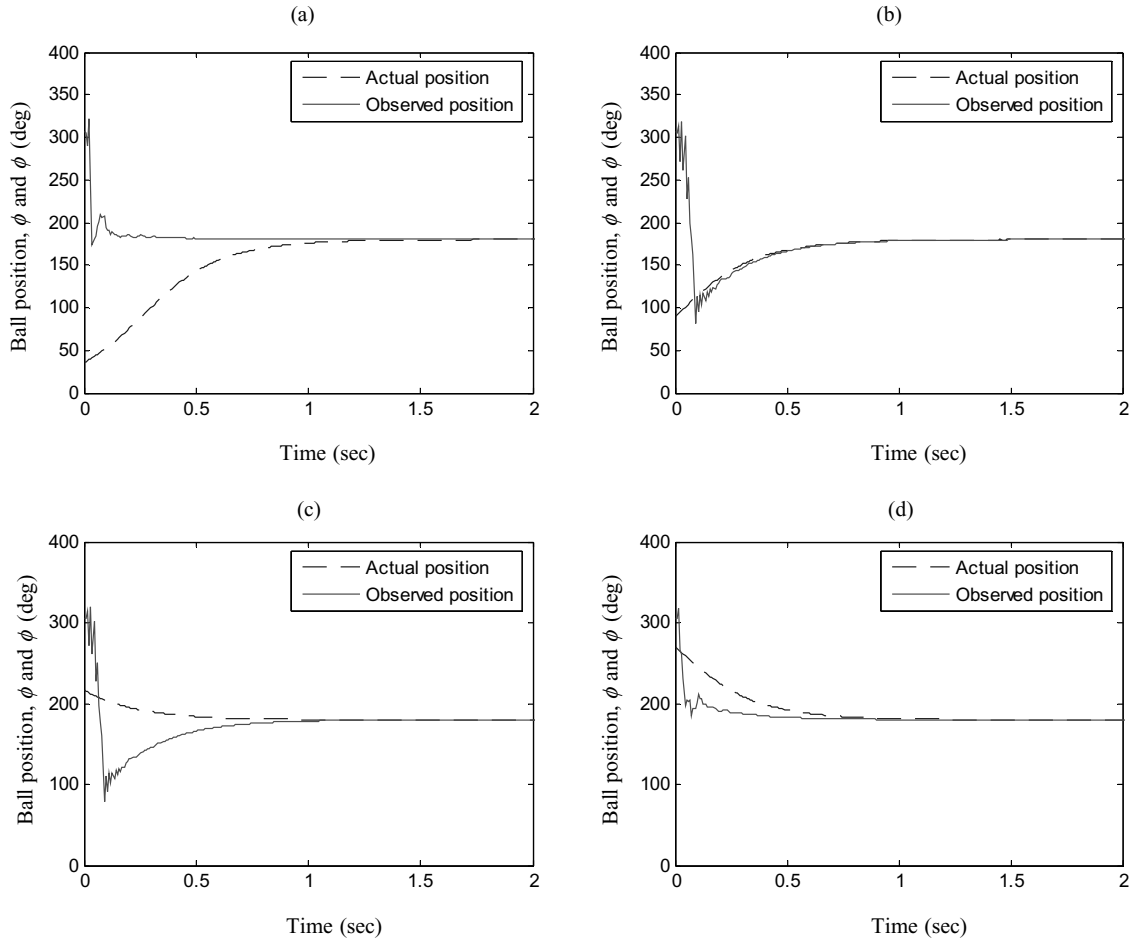

Fig. 11. Observed ball position based on the designed sliding-mode ball observer with $k_x = 460$, $k_x = 4$, $a_1 = 1$, $a_2 = 4$ and initial ball position at (a) 36°, (b) 90°, (c) 216° and (d) 270°.

and Y motions of the spindle-disc-ABS system. It is seen from Fig. 14(a) that the ball final positions in notations of stars are indistinguishable from 180 degree as viewed from the photo in Fig. 14(a), and also the positions observed by the sliding-mode ball observer are very close to 180 degree. Note that the experimental ball position can only be obtained at steady state since at transient period the position of the fast-rolling ball leaves a long blurry arc along its trace in the photos taken by the camera. It should also be noted at this point that due to the very small deviation of ball position from the exact 180 deg in practice, there still exist minor residual vibrations of the spindle-disc-ABS system along X and Y directions, which is evidenced from small steady-state oscillations at steady state in Fig. 14(b–i). Also seen from Fig. 14(b,f) are larger levels of vibration at the transient period before the ball settling to the 180 deg, which in some way validate the capability of the ABS to reduce the radial vibrations with the ball positioned around 180 deg at the steady state. As to verification of observer performance, it is seen from the aforementioned steady-state oscillations in Fig. 14(c,e,g,i) that the observed X and Y motions of the system closely follow the experimental counterparts, showing the effectiveness of the designed sliding-mode observer not only for ball position but also translational motions of the spindle-disc-ABS system along X and$Y$ directions.

5.2. Ball re-positioning via the proposed regulation scheme

Having validated the capability of the sliding-mode ball observer, the speed regulation scheme proposed in the end of Section 3.2 is utilized herein to re-position the ball to the desired position, 180 degree opposite to the inherent

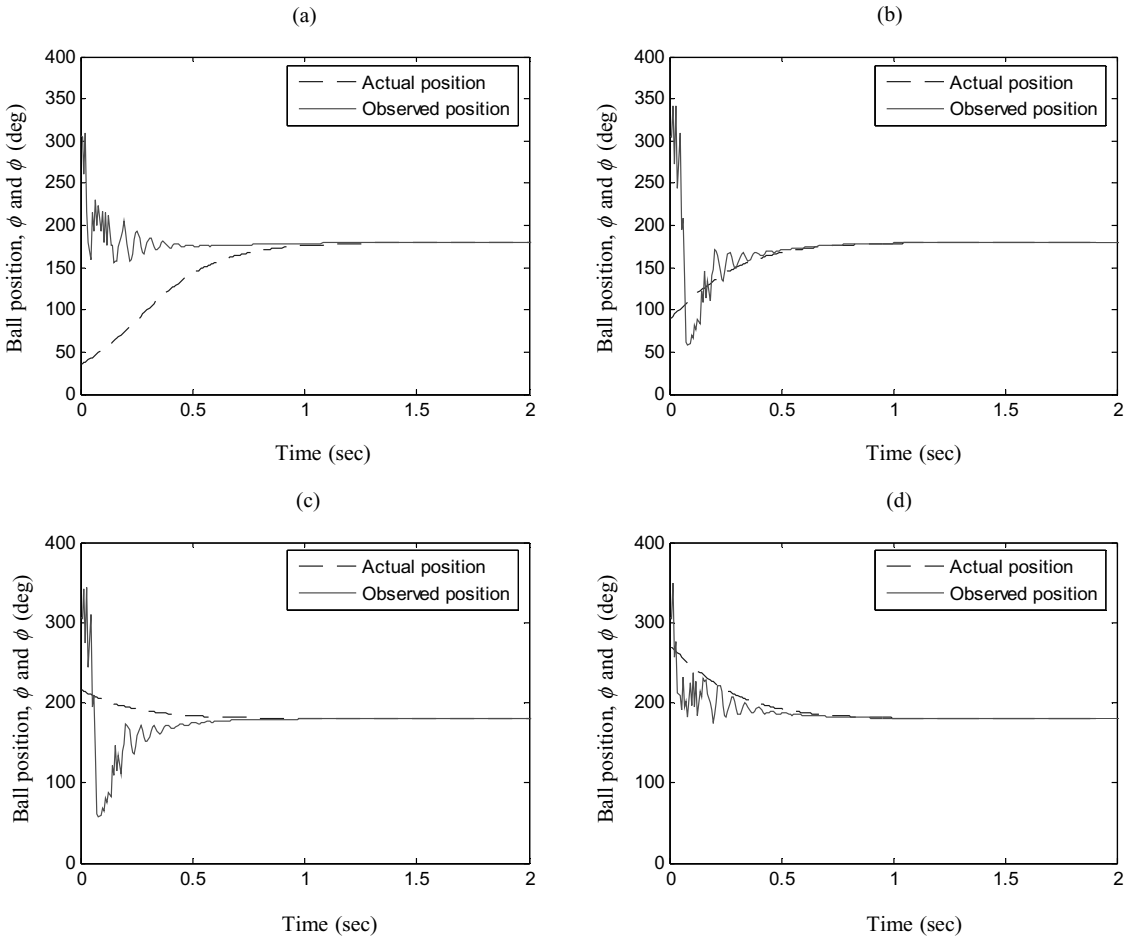

Fig. 12. Observed ball position based on the designed sliding-mode ball observer with $k_x = 460$, $k_x = 4$, $a_1 = 1$, $a_2 = 40$ and initial ball position at (a) 36°, (b) 90°, (c) 216° and (d) 270°.

imbalance of the spindle-disc-ABS system. As stated in Section 3.2, the regulator is designed to drop the spindle speed to the neighborhood of system's first translational resonance frequency, 1300 rpm, for several trials until the observed steady-state ball position is at 180 degree. Figures 15–17 show experimental results of the proposed regulation scheme with the target operation rotor speed as 2600 rpm, a low speed usually for writing mode. Figure 15 does the one with the ball positioned at the desired 180 degree with two trials while figure 16 with three trials. Also seen in Fig. 17 are the results with the target operation rotor speed set as 9000 rpm, a high speed for reading-mode of a large group of disc drives. It is seen from Fig. 15 that before the first trial the observed ball position is around -120 degree as the spindle speed first reaches the operational 2600 rpm. This observed -120 degree is close to the photographed -118 degree of the ball position as shown in Fig. 15(a). Since the ball does not reside at 180 deg, the trials of speed drops to approximate 1300 rpm are repeated two times to have the ball finally resided at 180 degree, as shown in Fig. 15(a). During the trials, the ball position estimated by the sliding-mode observer are shown close to those actual ball positions as photographed by the camera and shown in Fig. 15(a). Figure 16 presents another similar case where three trials are required to reside the ball at the 180 degree. Finally, Fig. 17 shows the case with a higher target speed as 9000 rpm, usually for reading mode, it is clearly seen from this figure that the proposed scheme is also capable of residing the ball at 180 deg after three trials of speed drops. Note that the continued success of residing the ball within limited number of speed-drop trials for higher target operation speeds results from the fact that the proposed scheme initiates and largely finishes ball re-positioning while the rotor speed is in the vicinity of suspension resonance (1300 rpm) not near the target operation speed.

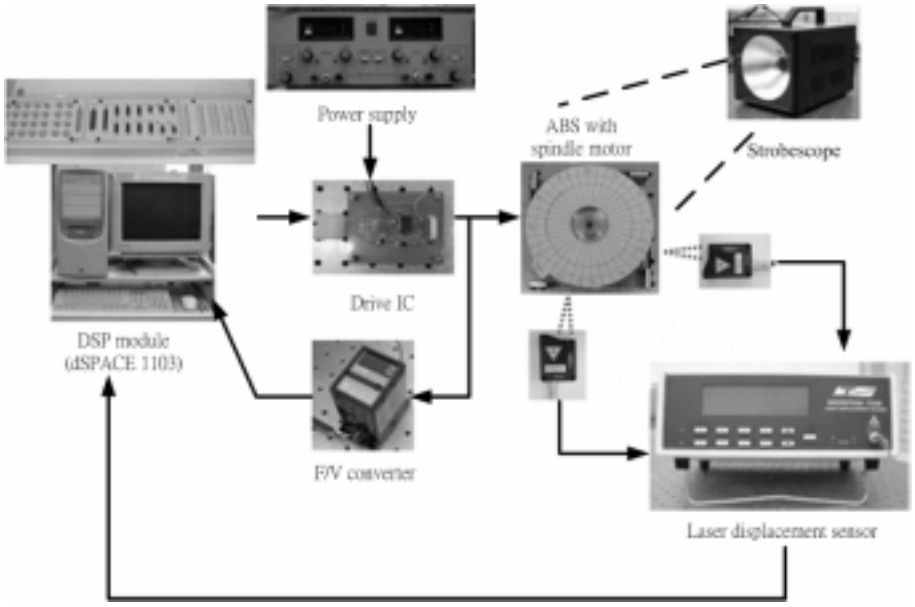

Fig. 13. Experimental setup.

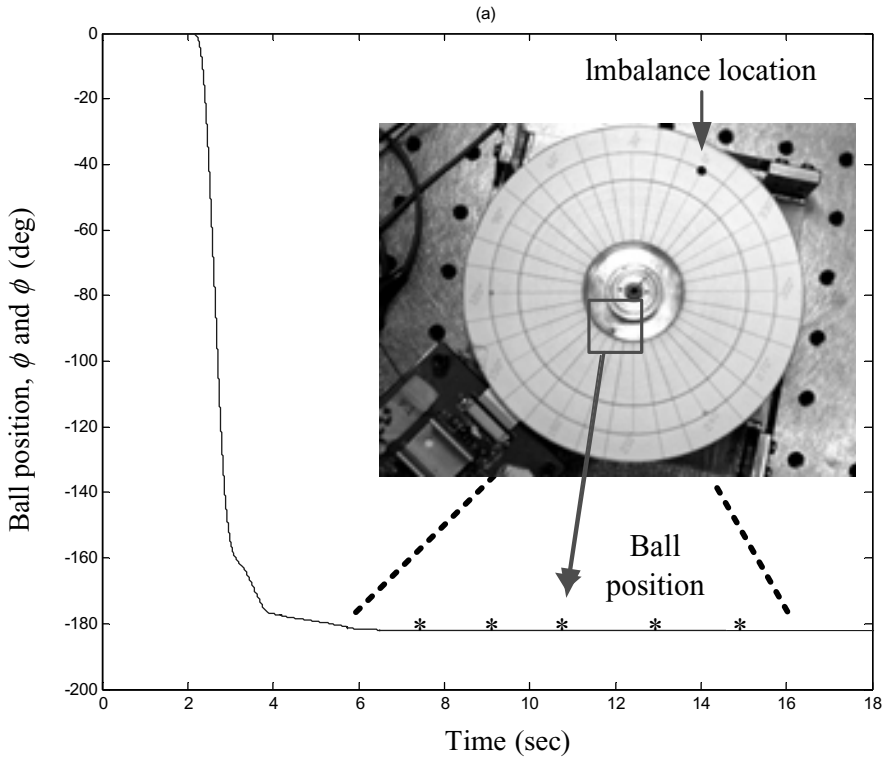

Fig. 14. (a) Observed ball position and the corresponding picture of ball position at steady state. (b) Measured and observed displacements of the stator and rotor system in X-axis. (c) The enlarged plot of Fig. 7(b) during a steady state period spanning 0.2 second. (d) Measured and observed velocities of stator and rotor system in X-axis. (e) The enlarged plot of Fig. 7(d) during a steady state period spanning 0.2 second. (f) Measured and observed displacements of stator and rotor system in Y-axis. (g) The enlarged plot of Fig. 7(f) during a steady state period spanning 0.2 second. (h) Measured and observed velocities of stator and rotor system in Y-axis. (i) The enlarged plot of Fig. 7(h) during a steady state period spanning 0.2 second.

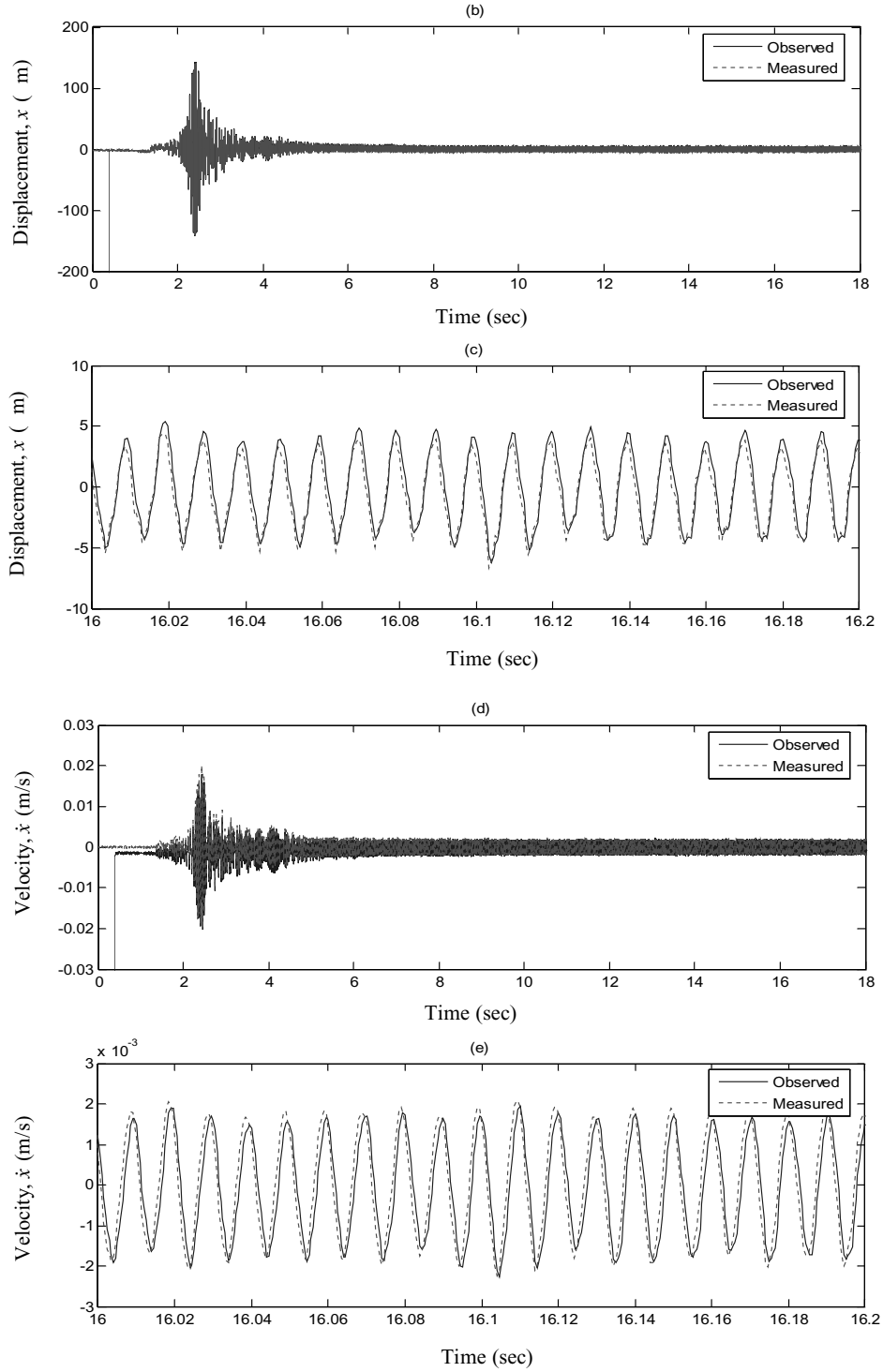

Fig. 14, continued.

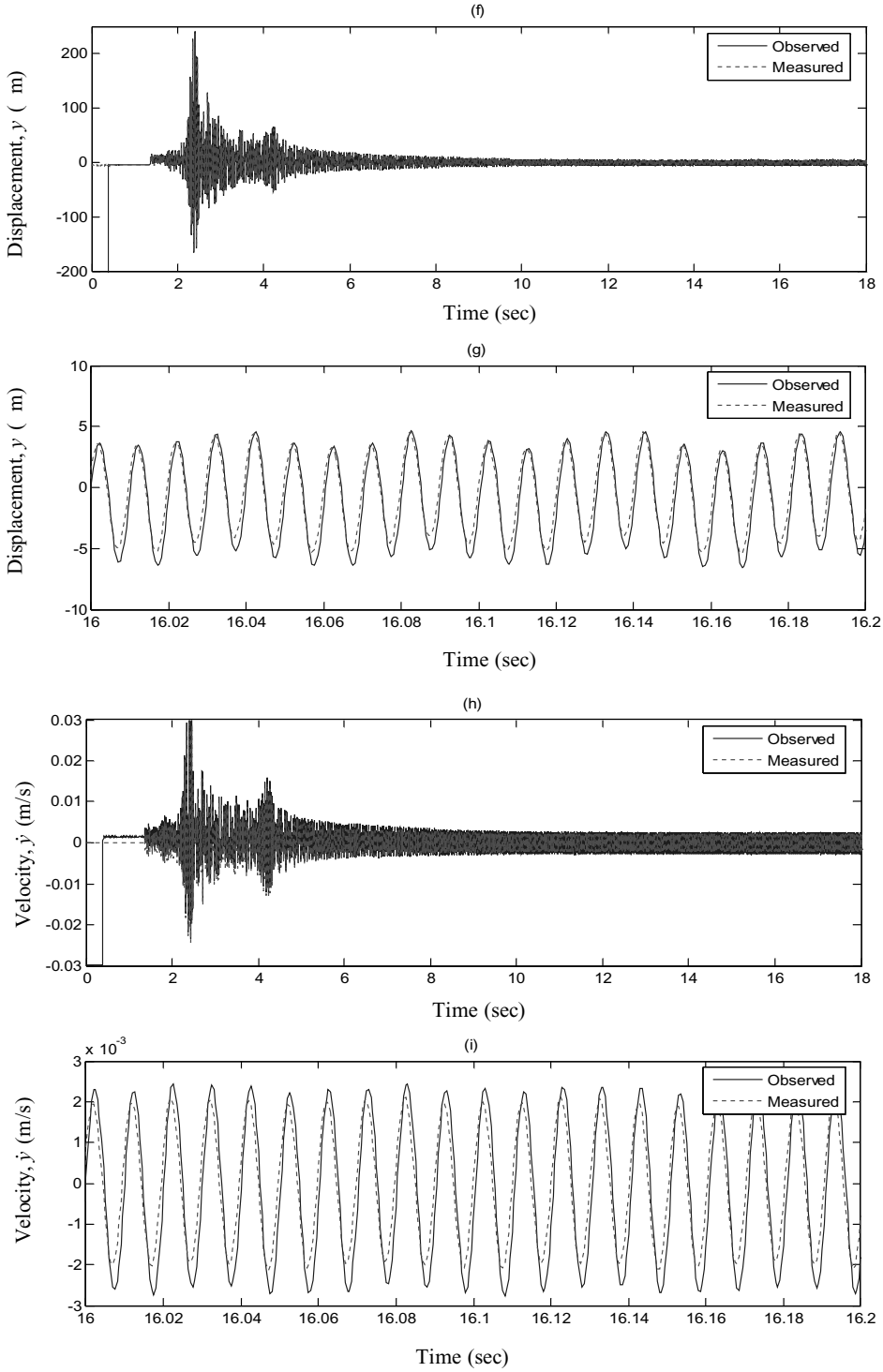

Fig. 14, continued.

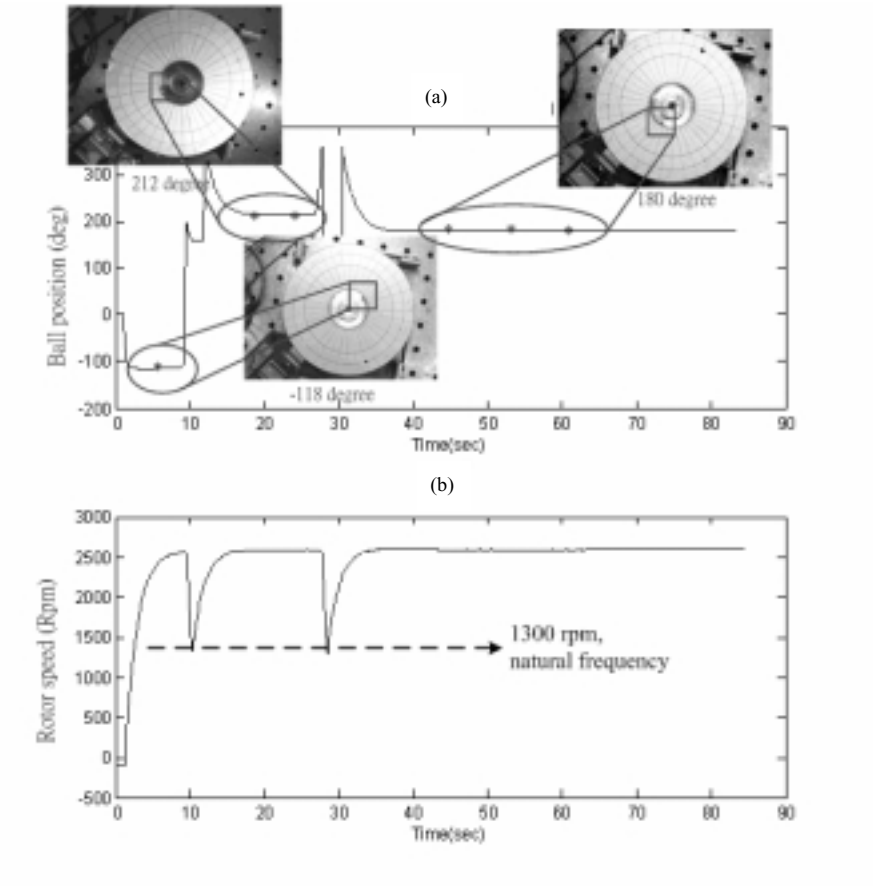

Fig. 15. Experimental results by the ball re-positioning scheme with operation speed 2600 rpm, experiencing two trials of speed drops. (a) Ball position versus time and the corresponding pictures, where the solid line, "–", represents the observed results and the stars, "*", denotes the actual ball positions. (b) The rotating speed of spindle motor versus time.

Based on the previous experimental results from executions of the speed regulation scheme, it can be perceived that the total number of trials for the ball to reside at the desired 180 degree probably depends greatly on the initial ball position and the rolling friction between the ball and ABS race flange. The rolling friction is, however, determined largely by the manufacturing precision and quality for the race, and usually a factor difficult to control in reality. The proposed regulation scheme guarantees only that through continuous trials of speed drop the ball stands for a fair chance to be resided at the desired 180 degree but not guaranteed. To fully understand the chance of ball residence at 180 deg against the practical races with varied rolling friction in continuous trials of speed drops, a study of executing the proposed regulation scheme 100 times with various initial ball positions are conducted for the case with operation speed as 2600 rpm. The results are summarized as pi charts in Fig. 18, where it seen that out of 100 times of regulation executions, 89% are able to reside the ball at the desired position within 5 trials while only the remaining 11% needs to reside the ball more than 5 trials. It demonstrates the satisfactory effectiveness of the proposed speed regulation scheme to re-position the ball. On the other hand, another pi chart in the same figure shows the distribution of number of trials for the aforementioned 89%, where it is seen that the case of three trials is most seen one as executing the regulation scheme.

6. Conclusions

A spindle speed regulation scheme assisted by a sliding-mode ball observer is successfully synthesized in this study to re-position the balancing ball inside the automatic balancer system (ABS) at the desired location. The

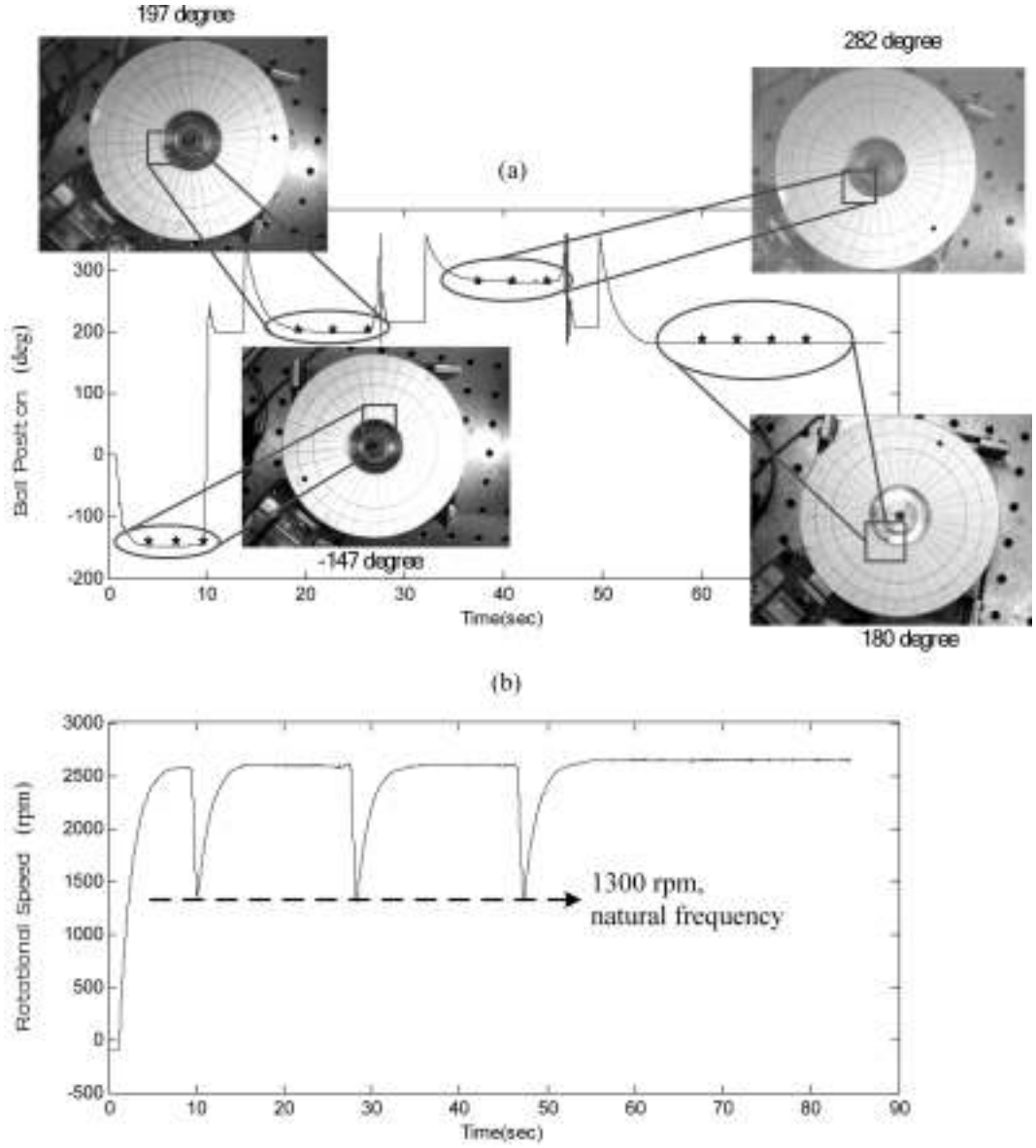

Fig. 16. Experimental results by the ball re-positioning scheme with operation speed 2600 rpm, experiencing three trials of speed drops. (a) Ball position versus time and the corresponding pictures, where the solid line, "–", represents the observed results and the stars, "*", denotes the actual ball positions. (b) The rotating speed of spindle motor versus time.

scheme consists of essentially a series of sudden drops in the spindle speed to the neighborhood of the first resonance frequency of system suspension such that the ball takes advantage of small ball-residing ranges near suspension resonance to overcome larger rolling friction at high rotor speeds. It is expected to accomplish the ball re-positioning at the desired 180 degree (opposite to the rotor imbalance) and then lead to a substantial vibration reduction. In the scheme, the sliding-mode observer plays a role of providing on-line estimated ball position for initiating speed-drops.

Simulations are successfully conducted based on the established system equations with the sliding-mode ball observer having the gains leading to a favorable observation convergence speed without notable chatterings. Experiments on the system with the designed sliding-mode ball observer and the spindle speed regulation scheme applied for ball re-positioning are performed to validate the effectiveness of the proposed scheme. Satisfactory closeness between simulations and experimental results are present for a certain run of the speed regulation, showing

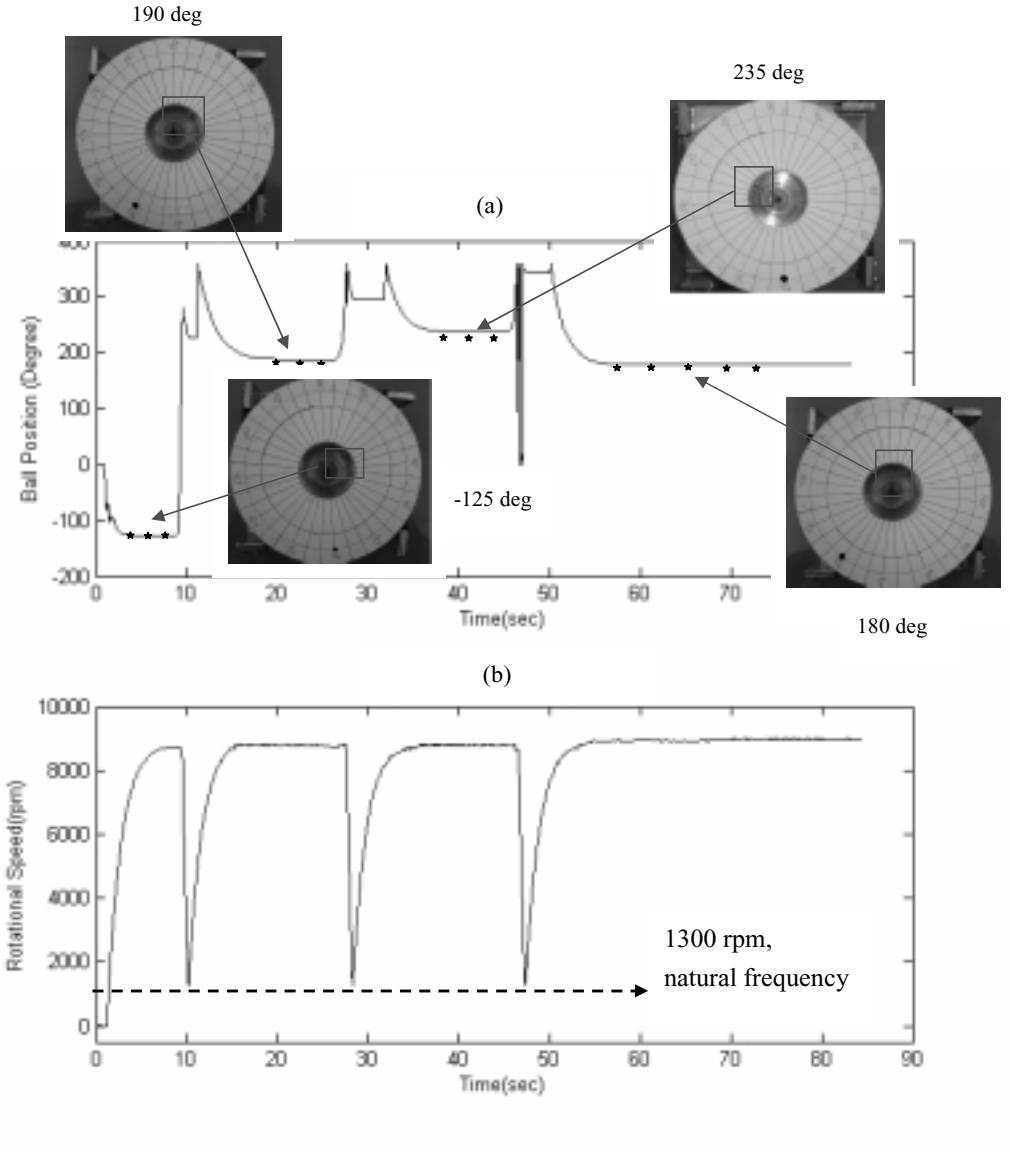

Fig. 17. Experimental results by the ball re-positioning scheme with operation speed 9000 rpm, experiencing three trials of speed drops. (a) Ball position versus time and the corresponding pictures, where the solid line, "–", represents the observed results and the stars, "*", denotes the actual ball positions. (b) The rotating speed of spindle motor versus time.

the effectiveness of the dynamic model, the sliding-mode ball observer and the proposed re-positioning scheme. Further experimental runs on the required number of trials to achieve the ball re-positioning at the desired 180 deg are conducted for the cases with low (2600 rpm) and high (9000 rpm) operation speeds. The results show that the proposed scheme is able to re-position the ball within reasonable number of speed-drop trials for both low and high speeds. This is found based on the fact that the proposed scheme initiates and largely finishes ball re-positioning while the rotor speed is in the neighborhood of suspension resonance, 1300 rpm, not near the target operation speed. On the other hand, the distribution of 100 runs for 2600 rpm in number of speed-drop trials are obtained and show that 89% of runs are able to reside the ball at the desired position within 5 trials while only the remaining 11% needs more than 5 trials. It demonstrates the satisfactory effectiveness of the proposed speed regulation scheme to re-position the ball. Furthermore, within the aforementioned 89% of runs where the ball re-position is achieved within 5 trials, the case of three trials is mostly seen one as compared to other numbers of speed-drop trials.

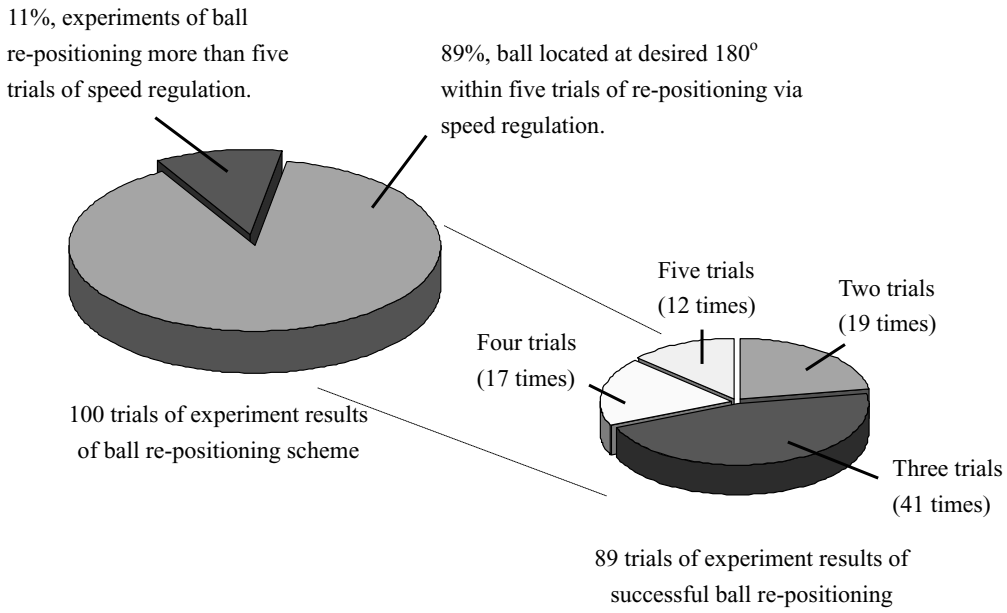

Fig. 18. Distribution of speed-drop trials via the low-torque speed regulator with operation speed at 2600 rpm.

Acknowledgement

The authors would like to pay special thanks to National Science Council of Republic of China for financially supporting this research project. The related contract nos. are NSC 94-2622-E-033-001 and NSC 94-2754-E-033-004.

Appendix A

The expressions of f_1 and f_2 are

$$f_1(\mathbf{x}, \boldsymbol{\phi}) = \begin{bmatrix} x_2 \; p_1 \; x_4 \; p_2 \end{bmatrix}^T,$$
$$f_2(\mathbf{x}, \boldsymbol{\phi}) = \begin{bmatrix} \phi_2 \; p_3 \end{bmatrix}^T,$$

where

$$\begin{aligned} p_1 = {} & \frac{1}{M}\{eM_R\dot{\theta}^2 - kx_1 - cx_2 + M(\dot{\theta}^2 x_1 + \ddot{\theta}x_3 + 2\dot{\theta}x_4) + mR[(\phi_2 + \dot{\theta})^2 \cos\phi_1 + \ddot{\theta}\sin\phi_1] \\ & - \frac{1}{m^2 - M(m + I/r^2)}[m\sin\phi_1(-\alpha_1 RM\phi_2 - MM_f sgn(\phi_2)/r + m^2 R\ddot{\theta} - mMR\ddot{\theta} \\ & + m(eM_R\ddot{\theta} + kx_3 + cx_4)\cos\phi_1 + m(eM_R\dot{\theta}^2 - kx_1 - cx_2)\sin\phi_1)]\}, \\ p_2 = {} & \frac{-1}{M}\{eM_R\dot{\theta}^2 + kx_3 + cx_4 + M(-\dot{\theta}^2 x_3 + \ddot{\theta}x_1 + 2\dot{\theta}x_2) - mR[(\phi_2 + \dot{\theta})^2 \sin\phi_1 - \ddot{\theta}\cos\phi_1] \\ & - \frac{1}{m^2 - M(m + I/r^2)}[m\cos\phi_1(-\alpha_1 RM\phi_2 - MM_f sgn(\phi_2)/r + m^2 R\ddot{\theta} - mMR\ddot{\theta} \\ & + m(eM_R\ddot{\theta} + kx_3 + cx_4)\cos\phi_1 + m(eM_R\dot{\theta}^2 - kx_1 - cx_2)\sin\phi_1)]\}, \\ p_3 = {} & \frac{1}{[m^2 - M(m + I/r^2)]R}\{\alpha_1 RM\phi_2 + MM_f sgn(\phi_2)/r - m^2 R\ddot{\theta} + mMR\ddot{\theta} \\ & - m(eM_R\ddot{\theta} + kx_3 + cx_4)\cos\phi_1 + m(-eM_R\dot{\theta}^2 + kx_1 + cx_2)\sin\phi_1\}. \end{aligned}$$

Appendix B

The expressions of **F**'s are as bellows.

$$\mathbf{F}_{11} = \begin{bmatrix} 0 & 1 & 0 & 0 \\ \dfrac{\partial p_1}{\partial x_1} & \dfrac{\partial p_1}{\partial x_2} & \dfrac{\partial p_1}{\partial x_3} & \dfrac{\partial p_1}{\partial x_4} \\ 0 & 0 & 0 & 1 \\ \dfrac{\partial p_2}{\partial x_1} & \dfrac{\partial p_2}{\partial x_2} & \dfrac{\partial p_2}{\partial x_3} & \dfrac{\partial p_2}{\partial x_4} \end{bmatrix},$$

where

$$\frac{\partial p_1}{\partial x_1} = \frac{1}{M}\left\{-k + M\dot{\theta}^2 + \frac{mk\sin\phi_1}{m^2 - M\left(m + I/r^2\right)}\right\},$$

$$\frac{\partial p_1}{\partial x_2} = \frac{1}{M}\left\{-c + \frac{cm\sin\phi_1}{m^2 - M\left(m + I/r^2\right)}\right\},$$

$$\frac{\partial p_1}{\partial x_3} = \frac{1}{M}\left\{M\ddot{\theta} - \frac{mk\cos\phi_1}{m^2 - M\left(m + I/r^2\right)}\right\},$$

$$\frac{\partial p_1}{\partial x_4} = \frac{1}{M}\left\{2M\dot{\theta} - \frac{mc\cos\phi_1}{m^2 - M\left(m + I/r^2\right)}\right\},$$

$$\frac{\partial p_2}{\partial x_1} = \frac{-1}{M}\left\{M\ddot{\theta} - \frac{mk\cos\phi_1}{m^2 - M\left(m + I/r^2\right)}\right\},$$

$$\frac{\partial p_2}{\partial x_1} = \frac{-1}{M}\left\{M\ddot{\theta} - \frac{mk\sin\phi_1}{m^2 - M\left(m + I/r^2\right)}\right\},$$

$$\frac{\partial p_2}{\partial x_2} = \frac{-1}{M}\left\{2M\dot{\theta} + \frac{mc\sin\phi_1}{m^2 - M\left(m + I/r^2\right)}\right\},$$

$$\frac{\partial p_2}{\partial x_3} = \frac{-1}{M}\left\{k - M\dot{\theta}^2 - \frac{mk\cos\phi_1}{m^2 - M\left(m + I/r^2\right)}\right\},$$

$$\frac{\partial p_2}{\partial x_4} = \frac{-1}{M}\left\{c - \frac{mc\cos\phi_1}{m^2 - M\left(m + I/r^2\right)}\right\}.$$

And

$$\mathbf{F}_{12} = \begin{bmatrix} 0 & 0 \\ \dfrac{\partial p_1}{\partial \phi_1} & \dfrac{\partial p_1}{\partial \phi_2} \\ 0 & 0 \\ \dfrac{\partial p_2}{\partial \phi_1} & \dfrac{\partial p_2}{\partial \phi_2} \end{bmatrix},$$

where

$$\frac{\partial p_1}{\partial \phi_1} = \frac{1}{M}\left\{-mR\left[\left(\phi_2 + \dot{\theta}\right)^2 \sin\phi_1 - \ddot{\theta}\cos\phi_1\right] - \frac{m}{m^2 - M\left(m + I/r^2\right)} * \right.$$
$$\left[\cos\phi_1\left(-\alpha_1 RM\phi_2 - MM_{f/r} + m^2 R\ddot{\theta} - mMR\ddot{\theta}\right)\right.$$
$$\left.\left.+m\left(\cos^2\phi_1 - \sin^2\phi\right)\left(eM_R\ddot{\theta} + kx_3 + cx_4\right) + m\sin 2\phi_1\left(eM_R\dot{\theta}^2 - kx_1 - cx_2\right)\right]\right\},$$

$$\frac{\partial p_1}{\partial \phi_2} = \frac{1}{M}\left\{2mR\cos\phi_1\left(\phi_2+\dot{\theta}\right)+\frac{\alpha_1 mRM\sin\phi_1}{m^2-M\left(m+I/r^2\right)}\right\},$$

$$\frac{\partial p_2}{\partial \phi_1} = \frac{1}{M}\left\{mR\left[\left(\phi_2+\dot{\theta}\right)^2\cos\phi_1+\ddot{\theta}\sin\phi_1\right]+\frac{m}{m^2-M\left(m+I/r^2\right)}\ *\right.$$
$$\left[-\sin\phi_1\left(-\alpha_1 RM\phi_2 - MM_{f/r}+m^2R\ddot{\theta}-mMR\ddot{\theta}\right)\right.$$
$$\left.\left.+m\left(\sin^2\phi_1-\cos^2\phi\right)\left(eM_R\ddot{\theta}-kx_1+cx_2\right)-m\sin 2\phi_1\left(eM_R\dot{\theta}^2+kx_3+cx_4\right)\right]\right\},$$

$$\frac{\partial p_2}{\partial \phi_2} = \frac{-1}{M}\left\{-2mR\sin\phi_1\left(\phi_2+\dot{\theta}\right)+\frac{\alpha_1 mRM\cos\phi_1}{m^2-M\left(m+I/r^2\right)}\right\}.$$

And

$$\mathbf{F}_{21} = \begin{bmatrix} 0 & 0 & 0 & 0 \\ \dfrac{\partial p_3}{\partial x_1} & \dfrac{\partial p_3}{\partial x_2} & \dfrac{\partial p_3}{\partial x_3} & \dfrac{\partial p_3}{\partial x_4} \end{bmatrix},$$

where

$$\frac{\partial p_3}{\partial x_1} = \frac{mk\sin\phi_1}{R\left[m^2-M\left(m+I/r^2\right)\right]},$$

$$\frac{\partial p_3}{\partial x_2} = \frac{mc\sin\phi_1}{R\left[m^2-M\left(m+I/r^2\right)\right]},$$

$$\frac{\partial p_3}{\partial x_3} = \frac{-mk\cos\phi_1}{R\left[m^2-M\left(m+I/r^2\right)\right]},$$

$$\frac{\partial p_3}{\partial x_4} = \frac{-mc\cos\phi_1}{R\left[m^2-M\left(m+I/r^2\right)\right]}.$$

And

$$\mathbf{F}_{22} = \begin{bmatrix} 0 & 1 \\ \dfrac{\partial p_3}{\partial \phi_1} & \dfrac{\partial p_3}{\partial \phi_2} \end{bmatrix},$$

where

$$\frac{\partial p_3}{\partial \phi_1} = \frac{m}{R\left[m^2-M\left(m+I/r^2\right)\right]}\left[\left(eM_R\ddot{\theta}+kx_3+cx_4\right)\sin\phi_1+\left(-eM_R\dot{\theta}^2+kx_1+cx_2\right)\cos\phi_1\right],$$

$$\frac{\partial p_3}{\partial \phi_1} = \frac{\alpha_1 RM}{R\left[m^2-M\left(m+I/r^2\right)\right]}.$$

References

[1] E.L. Thearle, Automatic dynamic balancers (Part 1 Leblanc balancer), *Machine Design* **22** (September 1950), 119–124.

[2] E.L. Thearle, Automatic dynamic balancers (Part 2 – Ring, Pendulum, Ball Balancers), *Machine Design* **22** (October 1950), 103–106.

[3] J. Inoue, Y. Jinnouchi and S. Kubo, Automatic balancers, *Trans the JSME* (Part C) **49** (1979), 2142–2148.

[4] P. Bövik and C. Högfors, Autobalancing of rotors, *J Sound Vibration* **111** (1986), 429–440.

[5] Y. Jinnouchi, Y. Araki, J. Inoue, Y. Ohtsuka and C. Tan, Automatic balancer (Static balancing and transient response of a multi-ball balancer), *Trans the JSME* (Part C) **59** (1993), 79–84.

[6] J. Chung and I. Jang, Dynamic response and stability analysis of an automatic ball balancer for a flexible rotor, *J Sound Vibration* **259**(1) (2003), 31–43.

[7] C. Rajalingham and R.B. Bhat, Complete balancing of a disk mounted on a vertical cantilever shaft using a two ball automatic balancer, *J Sound Vibration* **290** (2006), 169–191.
[8] A.N. Gorbenko, Stability of the rotor ball automatic balancing, *Problemy Prochnosti* **3** (2003), 120–129.
[9] W.Y. Huang, C.P. Chao, J.R. Kang and C.K. Sung, The application of ball-type balancers on radial vibration reduction of high-speed optic disk drives, *J Sound Vibration* **250** (2002), 415–430.
[10] J.R. Kang, C.P. Chao, C.L. Huang and C.K. Sung, The dynamics of a ball-type balancer system equipped with a pair of free-moving balancing masses, *ASME J Vibr Acous* **123** (2001), 456–465.
[11] C.-P. Chao, Y.-D. Huang and C.-K. Sung, Non-planar Dynamic Modeling and Analysis of an Automatic Balancer System Equipped with Multiple Balancing Balls, *Mechanism and Machine Theory* **38** (2003), 1289–1305.
[12] W. Kim, D.-J. Lee and J. Chung, Three-dimensional, modeling and dynamic analysis of an automatic ball balancer in an optical disk drive, *J Sound Vibration* **285** (2005), 547–569.
[13] P.C.-P. Chao, C.-K. Sung and H.-C. Leu, Effects of rolling friction of the balancing balls on the automatic ball balancer for optical disk drives, *ASME J Tribology* **127** (October 2005), 845–856.
[14] P.C.P. Chao, C.-K. Sung and C.-C. Wang, Dynamic analysis of the optical disk dives equipped with an automatic ball balancer with consideration of torsional motions, *ASME J Applied Mech* **72** (November 2005), 826–842.
[15] P.C.P. Chao, C.-K. Sung, C.-L. Huang and J.-S. Huang, Precision repositioning of the balancing ball in an auto-balancer system via a fuzzy speed regulator equipped with a sliding-mode observer, *IEEE Trans on Control Sys Tech* **13** (November 2005), 1107–1118.
[16] J.J. Slotine, J.P. Lyons and E.A. Misawa, On sliding observers for nonlinear systems, *ASME J Dynam Syst Meas* **109** (1987), 245–252.
[17] I. Husain, S. Sodhi and M. Ehsani, A sliding mode observer based controller for switched reluctance motor drives, *Conf Rec IEEE-IAS Annu Meeting* **1** (1994), 635–643.
[18] J. Adolfsson, *A study of stability using multiple correction masses,* Master thesis, Royal Inst. Thechnol., 1997.